SUPERCONDUCTING ELECTRON LINEAR ACCELERATORS AND RECIRCULATING LINACS

H.-D. Gräf and A. Richter
Darmstadt Technical University, Darmstadt, Germany

Abstract
As LEP reached the high-energy limit for electron–positron storage rings it was realized that linear accelerators, so-called linear colliders, would be the next generation of accelerators in high-energy physics. In nuclear physics the scheme of recirculating linacs dominates the scenario of accelerators producing continuous wave electron beams for coincidence experiments, while superconducting electron–positron accelerators in a certain energy regime offer a possibly superior alternative to normal conducting accelerators. Superconducting accelerator technology is presently the only choice for recirculating electron linacs at energies above 2 GeV. Both types, superconducting linacs and recirculating linacs, are analysed with respect to their special characteristics, and existing accelerators of both kinds are discussed.

1. INTRODUCTION

The properties of particle accelerators are always dictated by the special requirements of the experiments using their beam. Experiments in elementary particle physics usually require beam energies as high as possible, pushing the accelerators to their technical limits. Therefore elementary particle physics has for decades worked in the domain of circular accelerators and storage rings usually providing two beams of different particles that hit each other head-on in colliding beam experiments.

The obvious advantage of these accelerators is that non-interacting particles are not 'wasted', they are circulated again and only the energy lost due to synchrotron radiation has to be supplied by radio frequency (RF) cavities in the storage ring. Accelerators of this type provide fairly high beam currents (in the range of several mA) and thus a sufficient rate of events. However, there is a fundamental limit for storage rings set by the laws of electrodynamics: the energy loss per turn due to the emission of synchrotron radiation is inversely proportional to the radius of curvature of the particle trajectory, but proportional to the fourth power of γ, the relativistic Lorentz factor (the ratio of total energy to energy at rest). For electrons and positrons the Large Electron–Positron collider LEP II has reached this limit despite its impressive circumference of 27 km. Therefore, at least for light particles, the successors of the high-energy storage rings will be linear colliders: two linear accelerators (linacs) pointing at each other with their beams hitting head-on at almost unbelievably small cross sections, generated in sophisticated final focus systems.

Pioneering work on linear colliders was performed at SLAC, where the existing 50 GeV electron linac was modified to accelerate electron and positron beams of very much improved quality. Two arcs were added to enable head-on collisions between the electrons and positrons in a final focus arrangement.

To date, competitive design studies for electron–positron colliders in the energy regime up to 1 TeV have been completed for normal conducting linacs such as the Next Linear Collider (NLC, a joint American–Japanese effort), and for superconducting linacs such as the TeV Energy Superconducting Linear Accelerator (TESLA, a joint European–American effort). For superconducting accelerating cavities, the critical magnetic field of the material from which they are fabricated sets an upper limit to the achievable accelerating gradient. For niobium (still the most common material for superconducting cavities in electron accelerators) the gradient will be limited to some 50 MV/m. Therefore, for linear colliders considerably exceeding an energy of 1 TeV, normal

conducting cavities at very high frequencies may be chosen. A study of such a collider, the Compact Linear Collider (CLIC), using the two-beam accelerator technique at frequencies of 30 GHz and extremely high accelerating fields, is presently under way at CERN. It seems therefore that high-energy physics will need linacs in the near future.

In Section 2 superconducting electron linacs and their basic properties are discussed. Section 3 is devoted to the schemes and related properties of recirculating linacs. A variety of examples for both superconducting electron linacs and recirculating linacs is presented and discussed in Section 4 and followed by some concluding remarks.

2. SUPERCONDUCTING ELECTRON LINACS

Basically, electron linacs are simple devices since, due to their small rest mass ($mc^2 = 0.511$ MeV), electrons move at a speed close to the speed of light (c) once they have gained a kinetic energy of a few MeV (e.g. $\beta = v/c \geq 0.99$ for $E_{kin} \geq 3.1$ MeV). Therefore, in an electron linac (with the exception of its very front end where the electrons enter from the source) the accelerating structures (electromagnetic resonators oscillating at microwave frequencies) can all operate at the same phase velocity $v_{ph} = c$ in synchronicity with the speed of the electrons; they are therefore all identical in geometry. Since the topic of accelerating cavities is covered by several lectures (see the contributions by J. LeDuff and W. Wuensch in this report) we restrict ourselves here to considerations that apply to superconducting electron linacs and recirculating superconducting linacs in particular. For general information on superconducting accelerators we refer the reader to Ref. [1], and for the historical development of recirculating linacs to Ref. [2].

2.1 Why superconducting linacs?

The properties required of an accelerator designed for nuclear physics experiments are quite different than those of an accelerator for high-energy physics. In high-energy physics, it is most important to have as high an energy as possible available in the centre-of-mass system, thus colliding beam experiments are chosen. In addition the rate of events, dn/dt, has to be high enough to achieve significant results in a reasonable time. Since the event rate is equal to the product of the luminosity *L* (a property of the accelerator) and the cross section of the investigated reaction σ (a quantity given by nature), the accelerators have to produce high luminosities.

In nuclear physics (investigation of excitation and decay of nuclei, and properties and interaction of elementary particles in nuclear matter) it is commonly more important to have maximum luminosity rather than the highest possible energy. Therefore, the combination of a single beam hitting a fixed target is the usual choice in nuclear physics, since in this way luminosities can be reached that exceed those of colliding beams by three orders of magnitude. For modern experiments in nuclear physics there is one more important requirement: in order to optimize the ratio of truly coincident to accidentally coincident events, the time structure of the beam has to be as uniform as possible. Accelerators using electromagnetic fields at microwave (RF) frequencies always produce a beam consisting of bunches separated by at least one RF period.

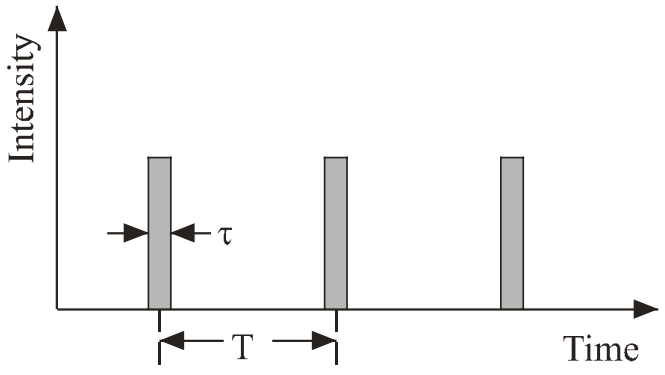

Fig. 1: Macroscopic time structure of a beam from a pulsed accelerator

Since the bunch repetition rate usually exceeds the maximum counting rate of the detectors by a long way, this so-called microstructure is neglected. If the accelerator is operated in a pulsed mode and produces (as indicated in Fig. 1) trains of bunches with a duration τ, separated by a time interval T, the macroscopic duty factor DF_{macro} of the beam is defined by $DF_{macro} = \tau/T$. If the accelerator produces a continuous train of bunches without any superimposed macrostructure, $DF_{macro} = 1$, the time structure is called Continuous Wave (CW). Continuous wave beams can either be achieved by expanding a pulsed beam in a stretcher ring, or naturally, by running the accelerator continuously. As will become clear in the following sections, the continuous operation of accelerating cavities at gradients of many MV/m is the natural domain of superconducting cavities.

2.2 Basic considerations

For an electric current oscillating at microwave frequencies, the surface resistivity of a superconductor does not vanish. According to BCS theory it has a finite value, depending on frequency and temperature. For temperatures below half the critical temperature of the superconductor ($T \leq T_c/2$) the surface resistivity R_s amounts to

$$R_s = A \cdot (f^{\kappa}/T) \cdot e^{-((\Delta/kTc)\cdot(Tc/T))} , \quad (1)$$

where f is the operating frequency (GHz), T the temperature (K), Δ the energy gap of the superconductor (eV), k the Boltzmann's constant, and T_c the critical temperature of the superconductor (K).

The quantities A and κ are usually determined experimentally. For niobium, which is still the only material in use for superconducting electron linacs (even in cavities with niobium sputtered on copper as is the case for most of the LEP cavities) values of $A = 9.0 \cdot 10^{-5}$ Ω K/(GHz)$^{\kappa}$, $\kappa = 1.9$, $\Delta/k\,T_c = 1.9$, and $T_c = 9.2$ K are found. Since the RF power dissipated in an accelerating cavity is proportional to R_s, Eq. (1) favours low operating frequencies (in contrast to normal conducting copper cavities), which unfortunately result in large cavities, cryostats, RF couplers, and other associated equipment. However, since the excitation of wakefields is very much reduced in cavities with large apertures, the final choice of the operating frequency will always be a trade-off between physics and financial considerations. In practice it has turned out that superconducting accelerating cavities for storage rings operate at frequencies below 1 GHz at temperatures of 4.2 K, whereas cavities for electron linacs operate in the range of 1.3–3 GHz at temperatures between 1.8–2 K. The fact that all superconducting accelerating structures operating in electron linacs are standing wave cavities is also a consequence of the low surface resistivity resulting from Eq. (1): the RF power dissipated in the cavity walls is only a small fraction of the power delivered to the beam and therefore, even in a pulsed application (as in a linear collider), the standing wave cavity has advantages over its travelling wave counterpart.

Beam dynamics in an electron linac is less complicated than in a circular accelerator. Longitudinally the electrons are synchronized to the phase velocity of the accelerating RF field and the electron bunches are usually positioned 'on crest' (at the maximum accelerating field) in order to minimize the effect of finite bunch length to energy spread (as discussed in Section 4.2, this can be different in recirculating linacs). The transverse focusing strength of the cavities (since they are standing wave cavities) is on the order of accelerating gradient/electron energy and is therefore only important at quite low energies. Quadrupoles, arranged in a FODO lattice, are the common choice for transverse beam optics, where in superconducting linacs they can either be positioned between or (in the case of very long cryomodules) inside cryogenic modules. In the latter case superconducting quadrupoles are used.

2.3 CW linacs: normal conducting vs superconducting

The following estimate of RF power, dissipated in a continuously running accelerating cavity, shows that it was the requirement for CW beams that led to the concept of recirculating linacs and in particular to superconducting recirculating linacs. The dissipated power P_{dis} per unit length (as sketched in Fig. 2) is given by

$$P_{dis} = E_{acc}^2/(R/Q)\cdot Q_0 , \quad (2)$$

where E_{acc} is the accelerating gradient, (R/Q) the normalized shunt impedance (depending on the geometry of cavity), and Q_0 the unloaded quality factor (depends on surface resistivity of material).

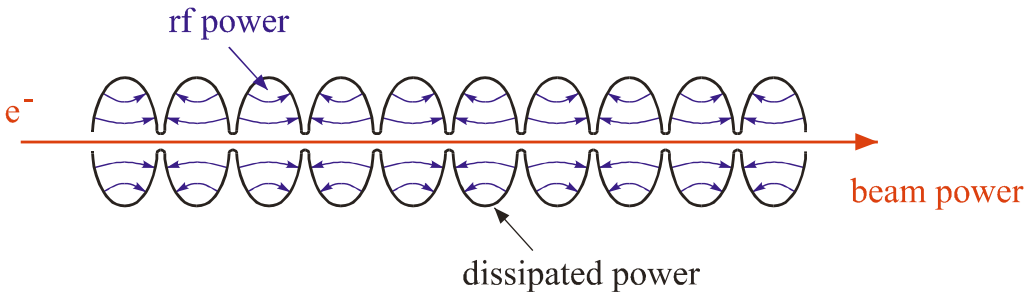

Fig. 2: Sketch of RF power distribution in CW linacs

Table 1 contains typical figures for well optimized normal conducting copper cavities and superconducting niobium cavities (both operating in S-band) as well as the dissipated power resulting from Eq. (2) for both cases.

Table 1: Comparison of typical S-band cavity parameters

Parameter	Normal conducting cavities	Superconducting cavities
(R / Q)	$4 \cdot 10^3$ Ω/m	$2 \cdot 10^3$ Ω/m
Q_0	$2.5 \cdot 10^4$	$3 \cdot 10^9$
E_{acc}	1 MV/m	5 MV/m
P_{dis}	10^4 W/m	4.2 W/m

Table 1 clearly indicates that the assumed gradient for normal conducting cavities is close to the technical limit and also that a linac, producing a beam of, for example, several hundred MeV would become unreasonably long.

For superconducting niobium cavities the small value of P_{dis} = 4.2 W/m indicates that gradients much higher than 5 MV/m are still reasonable. On the other hand, even at 10 MV/m a linac would still become very long. As a consequence, for both scenarios (normal conducting and superconducting linacs producing CW beams), a recirculating linac configured as described below is appropriate.

3. RECIRCULATING LINACS

The basic concept of a recirculating linac is that a beam of particles is accelerated several times in the same linac. Since the phase velocity of the accelerating field in the linac is fixed this scheme obviously only works for highly relativistic particles moving at velocities close to the speed of light, almost independent of their energy. Therefore, all the existing recirculating linacs are electron accelerators.

3.1 Basic schemes

The general layout of such a machine is indicated in Fig. 2. The accelerator consists of a linac placed between two ‘return devices’ (beam transport systems) that take the individual beams from the linac exit back to its entrance for the subsequent acceleration. (If the return devices are designed in such a way that the individual beams have a common return path between the two devices, a second linac can be placed there, essentially doubling the energy gain of the particles for each round trip in the accelerator; see for example the accelerator at the Thomas Jefferson National Accelerator Facility—TJNAF, or the fourth stage of the cascaded microtron MAMI C at Mainz, both discussed in Section 4.1). Two more devices are essential for a recirculating linac: one magnet system to inject the beam

from a source (usually an injector linac) into the recirculating linac and another magnet system for extraction of the beam after its final acceleration.

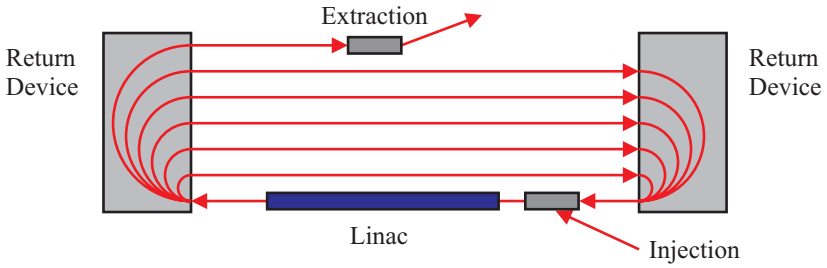

Fig. 2: Basic scheme of a recirculating linac

The final energy E_f of the recirculating linac is given by

$$E_f = N \cdot \Delta E_{linac} + E_{inj.} \,, \tag{3}$$

where N is the number of passes through the linac(s), ΔE_{linac} the energy gain in the linac(s), and E_{inj} the particle energy at injection.

Two basically different schemes exist for recirculating electron linacs: the polytron scheme and the scheme of 'independent orbit recirculation'. In a polytron a relatively small number of (large) dipole magnets forms the return devices. *All* of the recirculated beams pass through the same dipoles. The order of a polytron is usually indicated by an even number, p, which is equal to the number of dipoles. Each dipole bends the beams by an angle of $2\pi/p$. Figure 3 shows sketches of the lowest order polytrons, the racetrack microtron (p = 2), the double-sided racetrack microtron (p = 4), and the

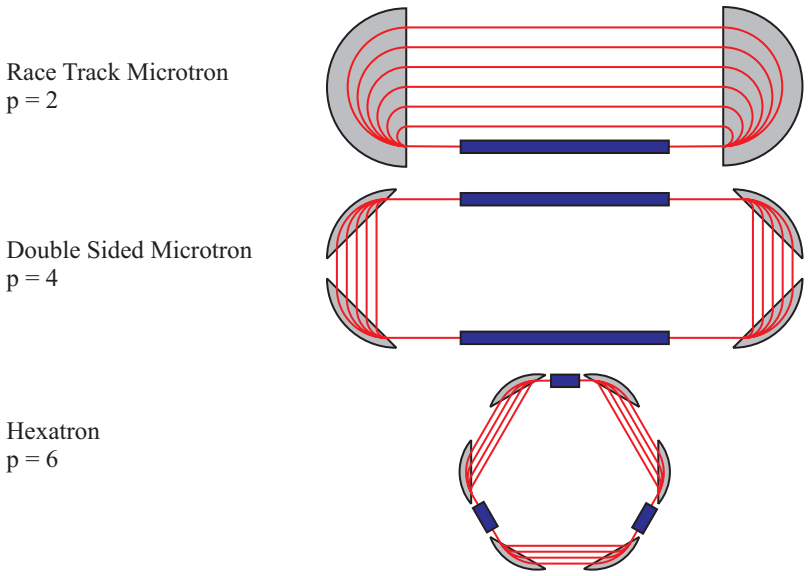

Fig. 3: Lowest order members of the 'polytron family'

hexatron (p = 6). The recirculating electron accelerator MAMI B at Mainz consists of three cascaded racetrack microtrons. A fourth stage is currently being developed and will be added to form MAMI C.

In a polytron, due to its high symmetry and the fact that the dipoles are common to all orbits, a relatively small number of parameters fixes the design of the accelerator. In a racetrack microtron (see Fig. 4 for a definition of quantities), two fundamental laws are obvious:

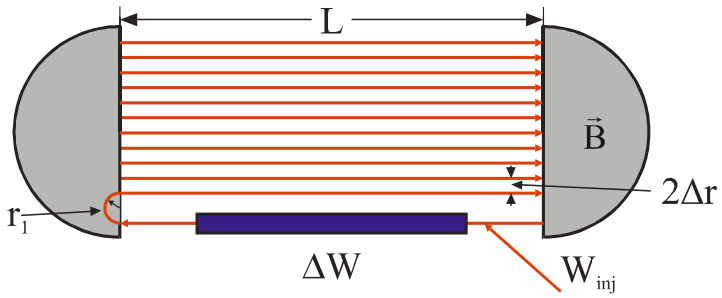

Fig. 4: Basic scheme of a racetrack microtron

i) the length of the first orbit must equal an integer number m of RF wavelengths λ $2\pi r_1 + 2L = m \cdot \lambda$, with r_1 being the radius of first orbit in dipole magnets and L the distance between dipole magnets;

ii) the length of each successive orbit must be longer than the previous orbit by an integer number ν of RF wavelengths λ
$2\Delta r = 2\pi\Delta W/ecB = \nu\lambda$, with 2Δr being the spacing of orbits, ΔW the energy gain in the linac, and B the magnetic field in dipoles.

As a consequence, once parameters ν and λ are chosen, the ratio of ΔW/B is fixed. Then selection of B fixes ΔW (or vice versa) and (for a given value of r_1) the injection energy. Finally, the number of recirculations, N, determines the size (weight and cost) of the dipole magnets.

The fundamentally different scheme of 'independent orbit recirculation' is sketched in Fig. 5. Here, many small dipole magnets are used in the return devices and, except for the splitters and recombiners (close to the entrance and exit of the linac), there are individual dipoles for each beam. The superconducting recirculating electron accelerators S-DALINAC at Darmstadt and the Continuous Electron Beam Accelerator Facility (CEBAF, the accelerator at the TJNAF) are examples of this scheme.

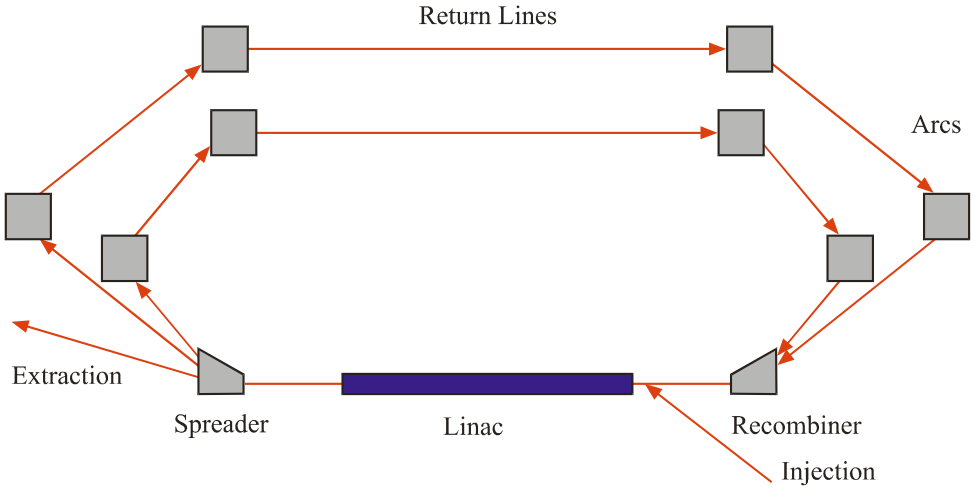

Fig. 5: Independent orbit recirculation

There is much more freedom in the design of the accelerator in the independent orbit recirculation scheme. Of course, the length of each orbit has to be equal to an integer number of RF wavelengths λ, but this number can be chosen independently for each orbit.

3.2 Efficiency of recirculating linacs

A brief analysis of the efficiency of recirculating linacs shows that different schemes are necessary for normal conducting and for superconducting linacs. Let η be the efficiency, defined as beam power divided by the electric power necessary to provide the RF power for acceleration. Then, for normal conducting linacs η is given by

$$\eta = (\eta_{rf} E_{acc} I_{beam} N)/[(E_{acc})^2/((R/Q)\, Q_0) + E_{acc} I_{beam} N] \,, \tag{4}$$

where η_{rf} is the power conversion efficiency (electric to RF), E_{acc} the accelerating gradient, I_{beam} the beam current, N the number of times the beam is accelerated in the linac(s), (R/Q) the normalized shunt impedance, and Q_0 the unloaded quality factor.

For superconducting linacs Eq. (4) has to be modified. The RF power dissipated in the accelerating cavities has to be taken away at a temperature of 1.8 or 2 K and thus must be divided by the efficiency η_{cryo} of the helium refrigerator, typically $\eta_{cryo} = 3.3 \times 10^{-3}$ for helium refrigerators of reasonable size. Then η is given by the expression

$$\eta = (\eta_{rf} E_{acc} I_{beam} N)/[(E_{acc})^2/((R/Q)Q_0)(1 + \eta_{rf}/\eta_{cryo}) + E_{acc} I_{beam} N]. \tag{5}$$

The result as shown in Fig. 6 is quite surprising, assuming $\eta_{rf} = 50\%$ and $\eta_{cryo} = 0.33\%$ for both types of accelerators, a beam current of 100 μA, and accelerating gradients of 1 MV/m and 5 MV/m for normal conducting and superconducting linacs, respectively. The normal conducting linac needs many recirculations in order to become effective (the upper limit of η is 50% since η_{rf} was chosen to be 50%!). This is the reason that the racetrack microtron configuration is very appropriate for normal conducting recirculating accelerators.

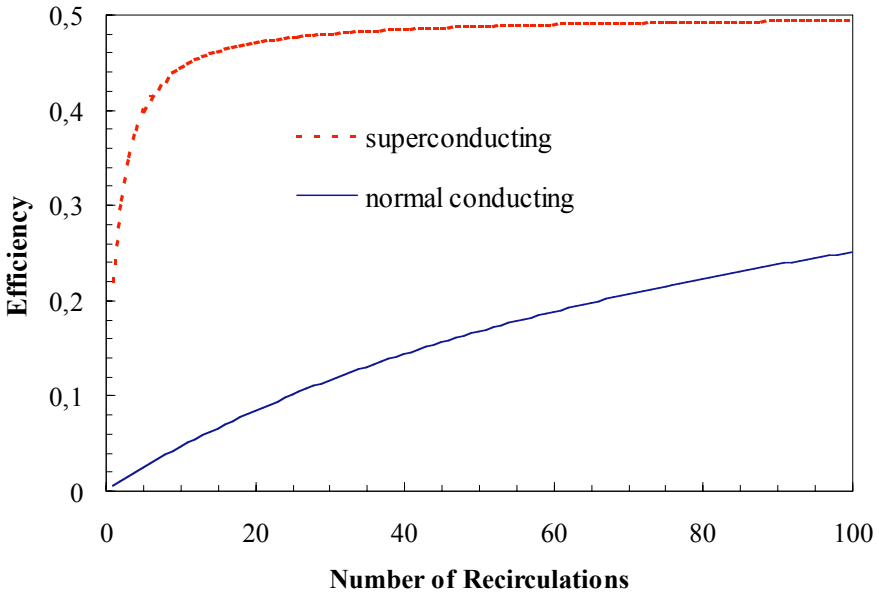

Fig. 6: Efficiency of recirculating linacs

The curve for superconducting accelerators (Fig. 6) shows that even a simple linac (N = 1) is effective and that a very small number of recirculations yields very good efficiencies. Superconducting recirculating electron linacs use recirculation schemes with independent optics on the individual recirculating beam lines.

3.3 Beam dynamics in recirculating linacs

In beam optics individual particles are described with respect to a reference particle that moves along the ideal trajectory with the correct longitudinal momentum p_0. For convenience a rectangular coordinate system x, y, z is used, whose origin moves along with the reference particle and whose z-axis is always tangential to the reference trajectory. Individual particles are then described in six-dimensional phase space by their spatial coordinates x, y, and z, and their corresponding momenta p_x, p_y, and p_z, or more commonly $\delta p_z = p_z - p_0$, the deviation from the correct longitudinal momentum. This characterization of individual particles is sketched in Fig. 7.

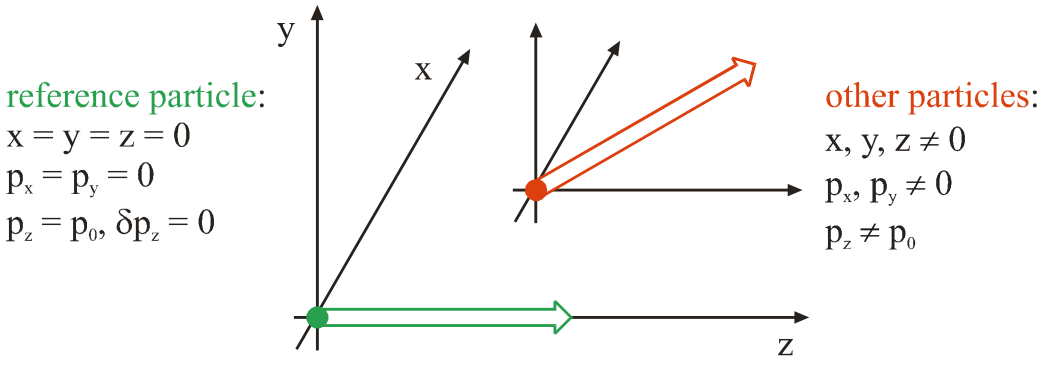

Fig. 7: Characterization of particles in phase space

In beam optics it is quite common for the inclination of the real trajectory with respect to the reference trajectory, given by $x' = p_x/p_0$ and $y' = p_y/p_0$, to be used instead of the transverse momenta. Whereas for the longitudinal coordinates the RF phase deviation ($\delta\phi = 2\pi z/\lambda$) and the relative momentum deviation ($\delta p_z/p_0$) are used. For particle ensembles suitable momenta of the whole ensemble have to be employed.

3.3.1 Longitudinal motion

The sketch in Fig. 8 illustrates the situation of a recirculating linac: particles are accelerated in the linac and after leaving it are returned to the entrance to be accelerated again. Even though the linac is always the same for each of the successive passes the energy gain of a particle (as indicated in the lower part of Fig. 8) depends on its phase with respect to the accelerating RF field, which in general will be different for each pass.

If φ_R denotes the correct phase of the reference particle, $\Delta W_R = eV_0 \cos(\varphi_R)$ is the correct energy gain for it. In general (for $\varphi \neq \varphi_R$) the energy gain ΔW will be $\Delta W = eV_0 \cdot \cos(\varphi_R + \delta\varphi) \approx eV_0 \cdot \cos(\varphi_R) - eV_0 \sin(\varphi_R)\delta\varphi = \Delta W_R + \delta W$. Since particle velocity and phase velocity of the RF field are assumed to be equal (very close to c) the phase deviation of the particle $\delta\varphi$ with respect to the reference particle remains unchanged. Thus, in a first order approximation, phase and energy deviation of a particle that enters the linac for the n^{th} time, $\delta\varphi_n$ and δW_n, transform into $\delta\varphi_{n+1}$ and δW_{n+1}, respectively, at the exit of the linac:

$$\begin{pmatrix} \delta\varphi_{n+1} \\ \delta W_{n+1} \end{pmatrix} = \begin{pmatrix} 1 & 0 \\ -\Delta W_R \cdot \tan(\varphi_R) & 1 \end{pmatrix} \cdot \begin{pmatrix} \delta\varphi_n \\ \delta W_n \end{pmatrix}. \tag{6}$$

In the case of the racetrack microtron the longitudinal properties of the returns are those of the two 180° dipole magnets (see Section 3.1). Therefore (again to a first order approximation) for the m^{th} passage of a particle through the return, phase and energy deviation transform in the following way:

$$\begin{pmatrix} \delta\varphi_{m+1} \\ \delta W_{m+1} \end{pmatrix} = \begin{pmatrix} 1 & 2\pi \cdot \nu / \Delta W \\ 0 & 1 \end{pmatrix} \cdot \begin{pmatrix} \delta\varphi_m \\ \delta W_m \end{pmatrix}. \tag{7}$$

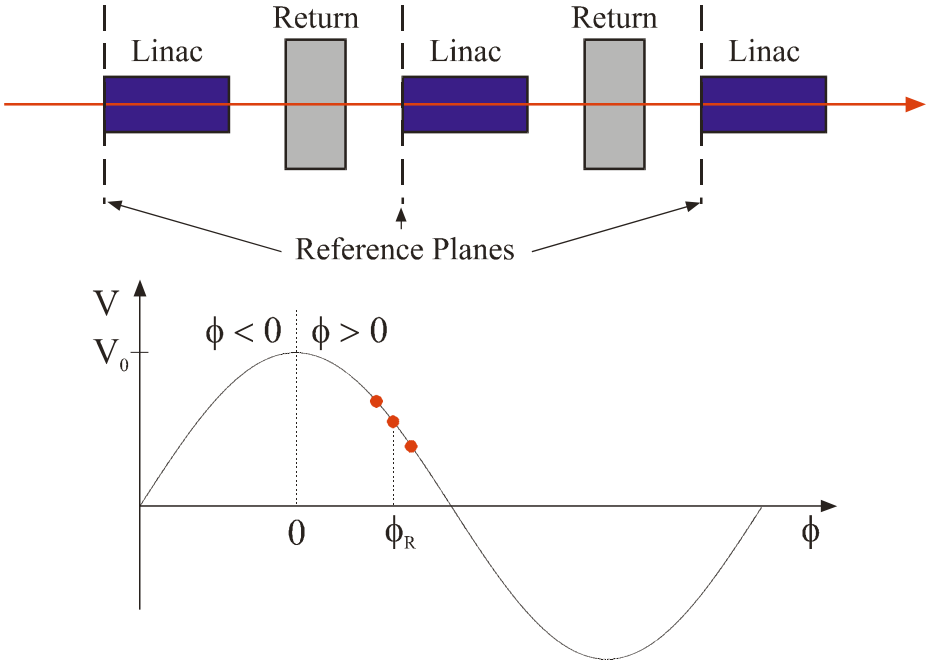

Fig. 8: Longitudinal motion

For a complete orbit (transport from one to the next reference plane in Fig. 8) first order transformation yields

$$\begin{pmatrix} \delta\varphi_{n+1} \\ \delta W_{n+1} \end{pmatrix} = \begin{pmatrix} 1-2\pi\cdot\nu\cdot\tan(\varphi_R) & 2\pi\cdot\nu/\Delta W \\ -\Delta W_R\cdot\tan(\varphi_R) & 1 \end{pmatrix}\cdot\begin{pmatrix} \delta\varphi_n \\ \delta W_n \end{pmatrix} \equiv \mathbf{M}\cdot\begin{pmatrix} \delta\varphi_n \\ \delta W_n \end{pmatrix}. \quad (8)$$

If the matrix **M** is the same for all orbits and Det(**M**) = 1 (conservation of phase space), the longitudinal motion of the particles is stable if Tr(**M**) < 2, i.e. the particles perform synchrotron oscillations in longitudinal phase space. The phase advance μ of these oscillations for one round trip in the racetrack microtron is defined by Tr(**M**) = 2 cos(μ). Using this definition of the phase advance μ, matrix **M** takes the general form

$$\mathbf{M} = \begin{pmatrix} \cos(\mu)+\alpha\cdot\sin(\mu) & \beta\cdot\sin(\mu) \\ -((1+\alpha^2)/\beta)\cdot\sin(\mu) & \cos(\mu)-\alpha\cdot\sin(\mu) \end{pmatrix}, \quad (9)$$

with α and β being constants.

Comparison of Eq. (9) with Eq. (8) gives the relation between phase advance μ and reference phase φ_R:

$$\cos(\mu) = 1 - \pi\nu\tan(\varphi_R) \ . \quad (10)$$

Considering that cos(μ) has to be less than one finally yields the condition for choosing φ_R such that the synchrotron motion of the particles in the recirculating linac is stable:

$$0 < \pi\nu\tan(\varphi_R) \ . \quad (11)$$

Independent orbit recirculation schemes are more flexible and allow for so-called isochronous designs, where the path length of the particles does not depend on the particle energy in the returns to first order approximation. In this case the recirculating linac is longitudinally equivalent to a straight single linac; the returns have no influence on the phase deviation of the particles. This situation is illustrated in Fig. 9 below.

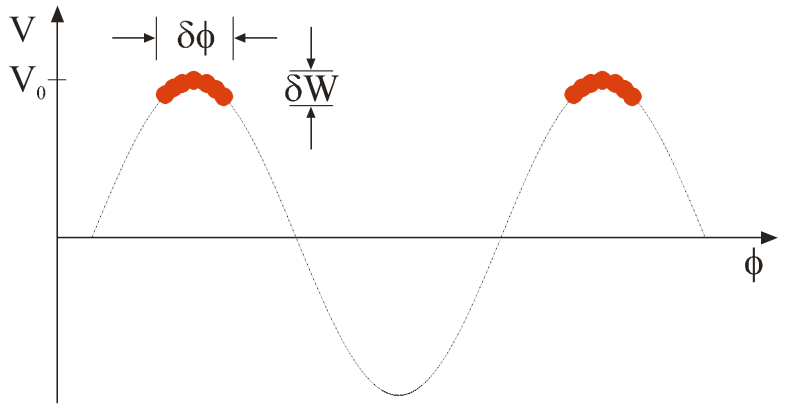

Fig. 9: Isochronous recirculation

In this scheme (neglecting all instabilities) the energy spread δW of the particles is determined by the bunch length δφ (see Fig. 9). Particles are usually accelerated 'on crest', using the accelerating field most efficiently. In this case the resulting energy spread δW is given by

$$\delta W = eV_0 \cdot (1 - \cos(\delta\varphi/2)) \approx eV_0 \delta\varphi^2/8 \; . \qquad (12)$$

and depends only to second order on the phase deviation δφ. However, since this scheme has no longitudinal stability the influence of any amplitude jitter or phase jitter of the accelerating field is not suppressed but fully reflected in the energy spread of the accelerated particle beam.

3.3.2 Transverse motion

In recirculating accelerators of the polytron type there are two possible schemes for achieving transverse stability. The first scheme, as sketched in Fig. 10, uses individual focusing on each return. The obvious advantage is that one can provide the same focusing strength for each orbit despite the increasing beam energy. However, there are two major disadvantages: the first is the large number of quadrupoles necessary and the second (possibly even more severe) is the fact that all quadrupoles are located in dispersive sections. This scheme of focusing on the individual returns has not been realized to date.

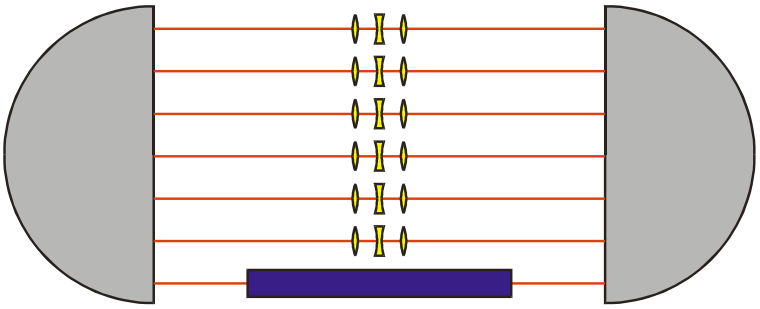

Fig. 10: First focusing scheme in a racetrack microtron

The second scheme, as indicated in Fig. 11, uses focusing elements only on the linac axis that is common to all orbits. Advantages of this method are first the very small number of quadrupoles needed, and second the fact that there is no dispersion on the linac axis, and therefore the quadrupoles do not influence the dispersive trajectory of the lattice. A disadvantage is the fact that the focusing strength decreases from orbit to orbit because of the steadily increasing beam energy. This finally leads to a limitation in the possible ratio of input to output energy ('Herminghaus condition': $W_{out}/W_{in} < 10$) for the racetrack microtron. This limitation in turn results in the configuration of multi-staged cascaded racetrack microtrons, where each stage can increase the beam energy by a factor of ten. The most successful examples of this type of recirculating linac are the cascaded racetrack microtrons of MAMI at Mainz, discussed in more detail in Section 4.

Fig. 11: Second focusing scheme in a racetrack microtron

The situation is completely different in machines that use independent orbit recirculation. There is (as indicated in Fig. 12 below) great flexibility in the layout of the lattice. Constraints are that the lattice has to be free of dispersion (or even isochronous) on the axis of the linac(s) and that it should also have no dispersion on the straight returns. One advantage of this scheme is the fact that magnets can be small (even the dipoles) since (except for spreaders and recombiners) they belong to individual orbits. Therefore, it is possible to place quradupoles in the arcs in locations with or without dispersion in order to tailor the optical properties of the lattice. On the straight return lines quadrupoles can be used either in a telescope-like imaging scheme or in a FODO arrangement.

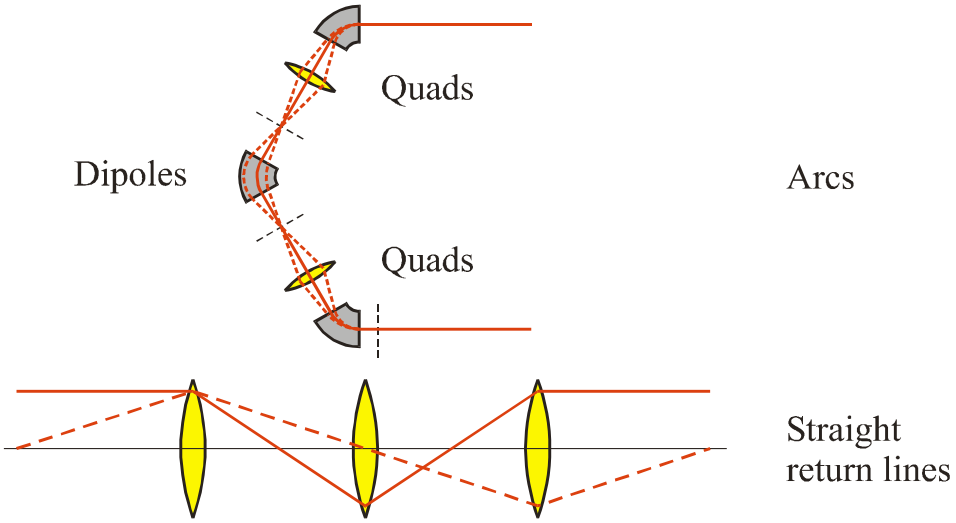

Fig. 12: Lattice schemes used in independent orbit recirculation

4. EXAMPLES

We now present in some detail examples of the different accelerator categories. The cascaded racetrack microtrons MAMI at Mainz have been chosen as a normal conducting recirculating electron linac since they display in a most beautiful way the features of this accelerator type (as explained in Section 3). Three examples of superconducting recirculating electron linacs are presented: the 130 MeV machine S-DALINAC at Darmstadt, the 5 GeV accelerator CEBAF at the TJNAF, and the proposed 25 GeV ELFE installation at CERN. Being a small installation, the S-DALINAC is best suited to looking into details of special features of this particular type of superconducting electron accelerator. CEBAF is the 'workhorse' operating at the high-energy end of CW electron accelerators in nuclear physics. It represents the biggest installation world-wide as far as the number of superconducting accelerator cavities is concerned. ELFE proposes to use the superconducting cavities of LEP II after its shutdown in a next-generation high-energy nuclear physics accelerator. Regarding superconducting electron linacs without recirculation, the installation of the TESLA Test Facility (TTF) at DESY and of course TESLA itself, the proposed 500 GeV electron–positron linear collider, are chosen. As examples of drivers of Free-Electron Lasers (FELs) the superconducting electron linacs of the S-DALINAC, the TTF, and the Infra Red Demonstration Free-Electron Laser (IR DEMO FEL)

at TJNAF have been selected. For detailed information on the individual accelerators we refer the reader to the Web pages of the respective institutes [3].

4.1 Recirculating linacs

4.1.1 MAMI at Mainz

Figure 13 shows the layout of the present accelerator installation MAMI B at Mainz (without experimental halls). It consists of two electron sources, a conventional (unpolarized) thermionic gun (labelled EKAN in Fig. 13) and a polarized source using a laser-driven strained GaAs photocathode (labelled PKA1). Both sources produce a 100 keV electron beam. A short injector linac (located between PKA1 and RTM1 in Fig. 13) with three RF structures increases the energy to 3.97 MeV. RTM1 is the first of the three cascaded racetrack microtrons of MAMI B. It uses one RF structure and 18 turns to increase the beam energy to 14.86 MeV. The second stage, RTM2, has two RF structures and in 51 turns the beam energy is increased to 180 MeV. The final stage, RTM3, has a linac consisting of five RF structures and the beam is recirculated as many as 89 times before it reaches its final energy of 855 MeV and is extracted to the experimental halls.

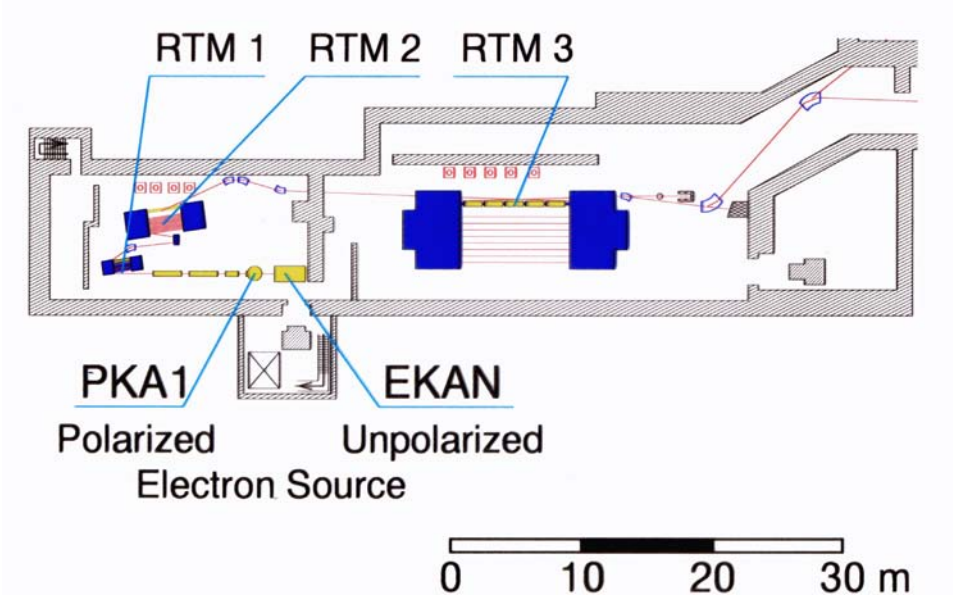

Fig. 13: Layout of MAMI B

Some of the most important parameters of the accelerators at Mainz are collated in Table 2. The data for the racetrack microtrons RTM1, RTM2, and RTM3 clearly display some of the particular features of this type of accelerator as discussed in Section 3. All three microtrons use the second focusing scheme (common focusing for all orbits on the linac axis) and Herminghaus' rule is only slightly violated in RTM2, where the ratio of output to input energy amounts to 12, rather than 10. One can derive the energy gain per RF structure from the number of turns and the number of RF structures contained in each linac. It amounts to 1.5–1.6 MeV (except for RTM1, where it is lower) and corresponds to $E_{acc} \approx 1$ MV/m, in agreement with the discussion of normal conducting accelerator cavities in Section 2.3. The exceptionally small energy spread (penultimate row of Table 2) is due to the longitudinal stability discussed in Section 3.3, inherent to the racetrack microtron scheme. Another salient feature of recirculating electron accelerators is also apparent in Table 2. The normalized emittances presented in the bottom row show a much stronger increase for the horizontal emittance than for the vertical emittance, due to the stochastic nature of synchrotron radiation. This effect requires that the number of recirculations should be kept low, particularly at energies approaching or exceeding 1 GeV, or in other words, for a given output energy the energy gain per turn should be high. This fact finally sets a limit on CW recirculating electron accelerators using normal conducting cavities.

Table 2: Collection of MAMI C parameters

Parameter	(Unit)	Injector	RTM1	RTM2	RTM3	HDSM
Energies	(MeV)	3.97	14.86	180	855	1500
Turns			18	51	90	43
Dipoles	(# / t)		2 / 2	2 / 45	2 / 450	4 / 250
Field	(T)		0.1026	0.555	1.284	1.53–0.95
Frequency	(GHz)	2.4495	2.4495	2.4495	2.4495	2.4495 / 4.899
RF structures		3	1	2	5	5 / 8
ΔE^a	(keV)	1.2	1.2	2.8	13	110
$\varepsilon_{x,n}/\varepsilon_{y,n}{}^a$	($\pi \cdot 10^{-6}$m)	0.05 / 0.04	0.07 / 0.07	0.25 / 0.13	13 / 0.84	27 / 1.2

[a] 1σ values

A fourth microtron is currently under construction at Mainz as an energy upgrade from 855 to 1500 MeV (conversion from MAMI B to MAMI C). It is not a racetrack microtron but rather a double-sided microtron (DSM). This is for two main reasons: first, as stages RTM1 to RTM3 show, the magnet weight for 180° dipole magnets would become excessive at 1500 MeV; second, since a DSM has a common axis for the beam return lines a second linac can be placed there and double the energy gain per turn. Finally, careful design studies revealed that a significant increase in longitudinal stability can be achieved if one of the two linacs operates at the first harmonic of the fundamental RF frequency of 2.4495 GHz. The resulting configuration therefore is called a Harmonic Double-Sided Microtron (HDSM).

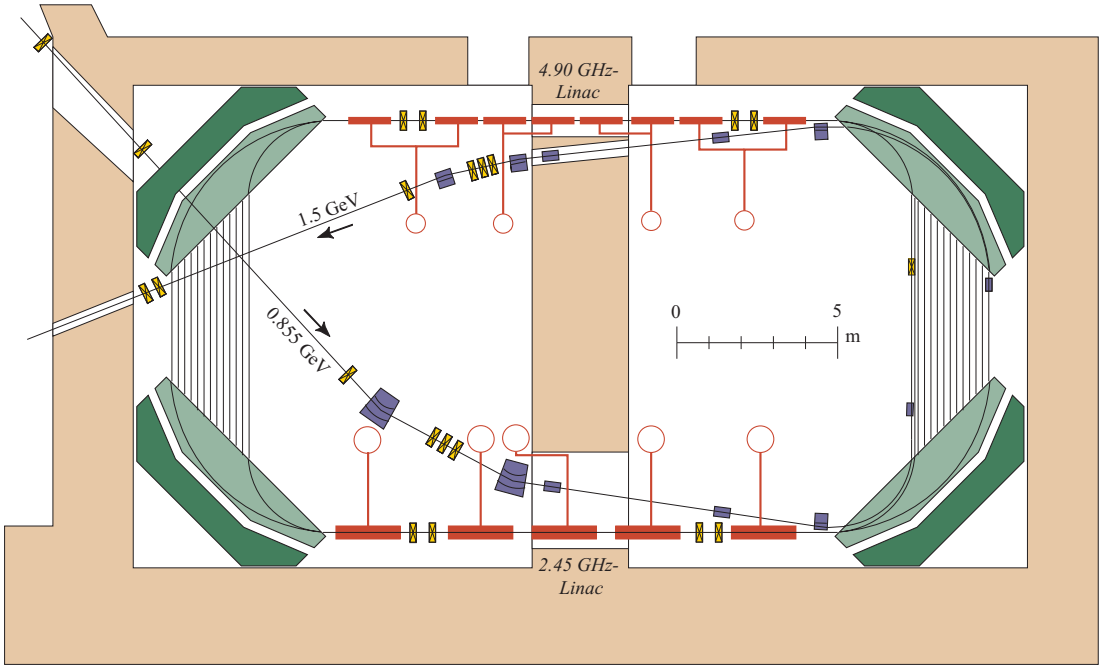

Fig. 13: Layout of the harmonic double-sided microtron (HDSM) at Mainz

The last column of Table 2 displays some of the notable data for the HDSM, and its layout is shown in Fig. 13. A look at the area covered by the four dipole magnets shows that, compared with a racetrack microtron, some 60% of magnet weight could be saved in the HDSM. The obvious drawback of the configuration, the strong focusing of the inclined magnet edges, is compensated by a

carefully tailored non-uniform field in the dipoles. Since the ratio of output to input energy is less than two, the focusing of the 43 beams is realized on both linac axes (the second focusing scheme). The harmonic 4.899 GHz linac consists of eight, and the fundamental 2.4495 GHz linac of five, RF structures; thus, both linacs have about the same physical length. Due to its compactness the HDSM fits into one of the existing experimental halls.

4.1.2 S-DALINAC at Darmstadt

Historically the S-DALINAC was the third superconducting recirculating electron accelerator after the racetrack microtron at the University of Illinois and the recirculating linac at Stanford University. Because of the advances in the design and fabrication of superconducting accelerating cavities that had been achieved at the time of its design and construction the S-DALINAC could be considered as a pilot project for its big brother CEBAF (discussed in the following subsection). The S-DALINAC's principle of operation is illustrated by its layout, shown in Fig. 15.

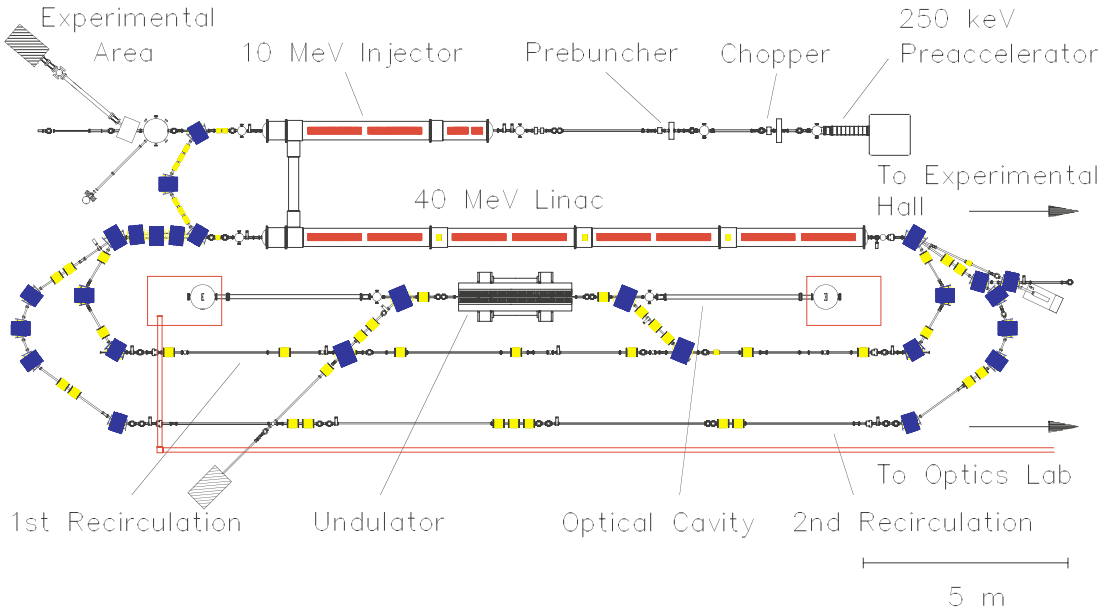

Fig. 15: Layout of the S-DALINAC

The electron source is located on a high-voltage terminal (top right) at 250 kV. The electrostatically preaccelerated beam receives its 3 GHz time structure, which is necessary for successive acceleration in the superconducting cavities to the chopper–prebuncher section at room temperature. The DC current from the source is first chopped into 30 ps long packages, which are then bunched to a length of 5 ps when they enter the superconducting injector linac. Acceleration is achieved by a 2-cell capture cavity ($\beta = 0.85$) followed by a 5-cell capture cavity ($\beta = 1.0$) and two 20-cell cavities, all fabricated from RRR = 280 niobium and operated in liquid helium at 2 K. When leaving the injector, the beam has an energy of up to 10 MeV and can either be used for low-energy experiments in an experimental area straight ahead or can be bent by 180° for injection into the main linac. There, eight 20-cell cavities (originally designed at the University of Wuppertal) installed in four identical cryomodules increase the beam energy by up to 40 MeV. When leaving the main linac the beam can either be extracted to the experimental hall or recirculated and reinjected one or two times by the appropriate beam transport systems (lower part of Fig. 16). The maximum beam energy after three passes through the main linac therefore amounts to 130 MeV. The central part of Fig. 15 shows the arrangement of the FEL. There, the beam from the straight section of the first recirculating beam line is bent over and passed through the undulator and then is either dumped or reinjected into the first recirculation for energy recovery experiments. Two mirrors to the left and right of the undulator form the 15 m long optical cavity. The evacuated transfer tube of some 50 m in length, for the radiation generated in the optical cavity, is indicated in the lower part of Fig. 15. Table 3 summarizes the most important parameters of the S-DALINAC.

Table 3: Design parameters of the S-DALINAC

Beam energy	130 MeV
Energy spread	$\pm 10^{-4}$
Beam current	20 μA
Duty cycle	CW
Cavity material	Niobium (RRR = 280)
Frequency	2.9975 GHz
Temperature	2 K
Quality factor	$3 \cdot 10^9$
Accelerating gradient	5 MV/m
RF losses at 5 MV/m	4.2 W/m

Fig. 16 shows a photograph of a 3 GHz superconducting 20-cell cavity. The cavity is a very slim object and, since high purity niobium is a rather soft material, cleaning, handling, and assembly of such cavities are delicate operations.

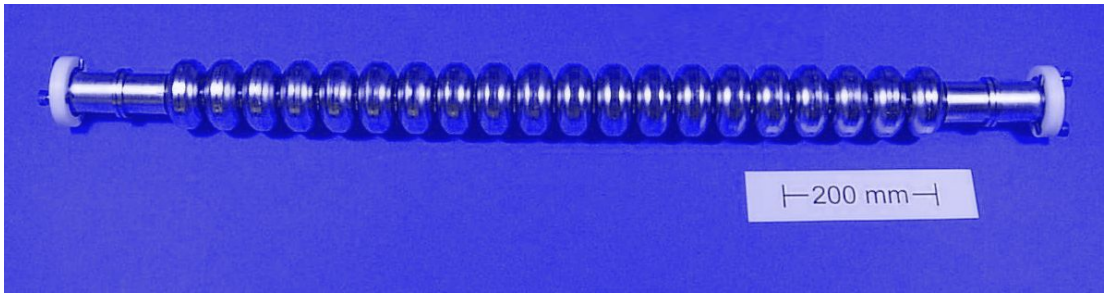

Fig. 16: Superconducting 3 GHz 20-cell cavity

All the cavities installed in the S-DALINAC clearly exceed the design gradient of 5 MV/m, averaging 6.7 MV/m. The only remaining drawback is the fact that the unloaded quality factors Q_0 are lower than the expected value of 3 x 10^9. The present average amounts to 7.7 x 10^8, resulting in increased dissipated RF power at 2 K. Since the helium refrigerator of the entire accelerator has only a capacity of slightly less than 120 W at 2 K it is the dissipated RF power that has up to now limited the maximum beam energy to 120 MeV. Therefore work continues on the improvement of Q_0 by, for example, applying new surface preparation techniques and the development of improved magnetic shielding.

The RF input couplers are very important parts of a superconducting accelerator and usually delicate. They have to transfer to the cavity the RF power necessary to achieve the correct gradient and accelerate the beam current. Since in superconducting cavities the wall losses are usually much smaller than the RF power transferred to the beam, the cavity represents a load that very much depends on the beam current, i.e. the transition from the RF input coupler to the cavity can change from being matched to being almost fully reflective. Thus one tries to optimize the input coupler in such a way that for maximum beam current (minimum loaded Q of the cavity) there is a minimum of reflected RF power (maximum power transfer efficiency). In this case the external quality factor (Q_{ext}) as presented by the input coupler, RF transfer line, and transmitter, equals the loaded Q of the cavity. Usually one defines the input coupling factor, or input coupling strength β_1, as the ratio Q_0 / Q_{ext}. Then the reflected power P_{refl} in terms of the forward power P_{forw} is given by by the following expression:

$$P_{refl} / P_{forw} = (1 - \beta_1)^2 / (1 + \beta_1)^2 . \qquad (13)$$

Figure 17 indicates how much forward RF power is needed for the S-DALINAC 20-cell cavities to accelerate different beam currents at a gradient of 5 MV/m as a function of the input coupling strength.

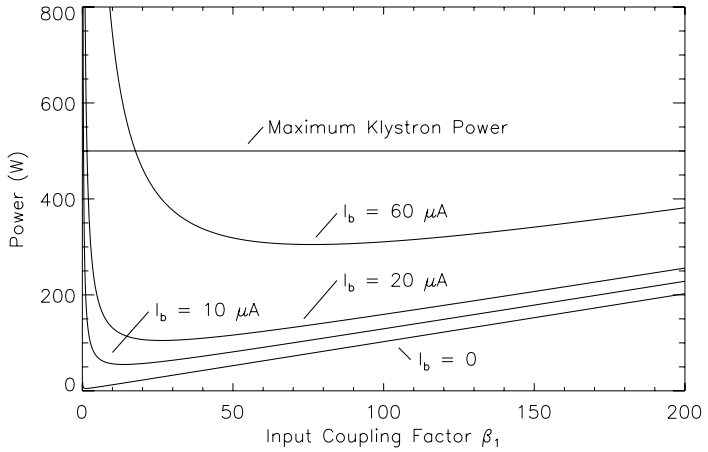

Fig. 17: Input coupling characteristics for the S-DALINAC 20-cell cavities at 5 MV/m

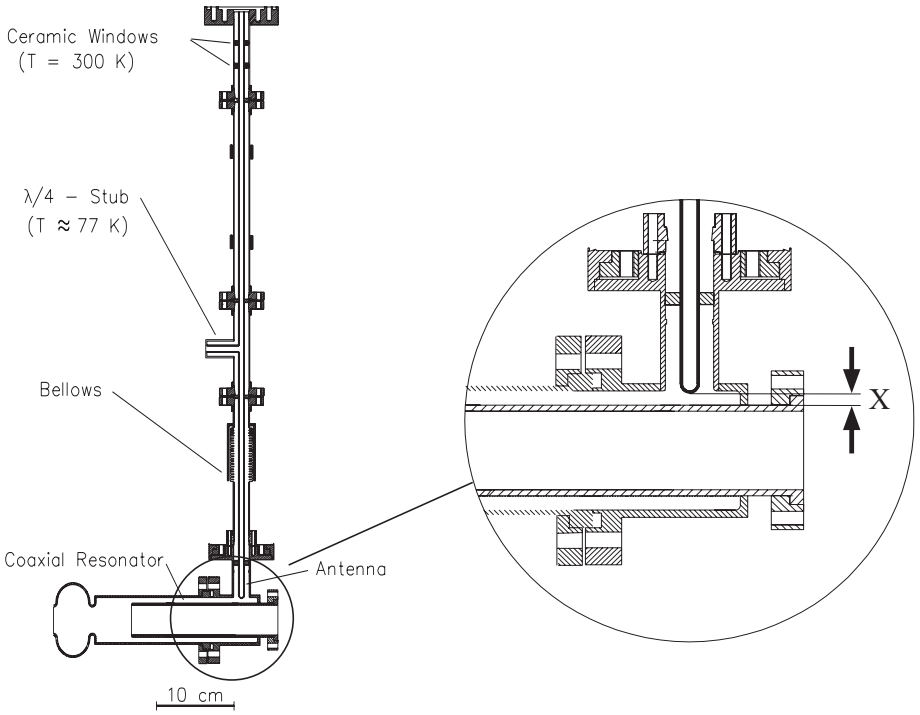

Fig. 18: Variable superconducting RF input coupler

For each beam current the corresponding curve has a minimum for a certain value of β_1 (matched condition), which increases with increasing beam current. Since the slope of all curves towards stronger coupling is less steep than for the undercoupled case it is common to use a little overcoupling. For diagnostic purposes, however, it is quite often desirable to match to the unloaded Q of the cavity (without beam) in order to obtain a resonance of minimum width and thus maximum diagnostic sensitivity.

The RF input couplers in the S-DALINAC allow for this option: they provide variable coupling strength over a wide range. The left part of Fig. 18 shows a cross section of the coupler with its coaxial RF input line. The interior of this line is common to the beam vacuum and is therefore sealed with two ceramic windows at room temperature (the volume between the two windows is common to

the insulating vacuum of the cryostat). Heat flow into the helium bath is minimized by the λ/4-stub, which is thermally connected to a liquid nitrogen cooled reservoir at 77 K. Transfer of RF power from the input line to the cavity is accomplished in two steps: the coaxial line couples to the coaxial resonator (lower part of Fig. 18), which in turn couples to the cavity (indicated by its first cell). Coupling between the coaxial line and resonator is determined by the distance x (right part of Fig. 18), which can be varied by shifting the top part of the coaxial line vertically while keeping the position of the coaxial resonator fixed. This is possible because of the bellows incorporated in the outer conductor of the coaxial line. The resulting variation in the overall coupling strength, expressed in terms of the external quality factor, is impressive and is shown in Fig. 19, which displays a measurement at 2 K (left part). It is clear that in situ diagnostic measurements at $Q_{ext} \approx 10^9$ (right part of Fig. 19) are possible with this coupler. Of course optimum matching to different beam loading conditions at $Q_{ext} \approx$ a few 10^7 is also possible by adjusting the input coupling strength accordingly.

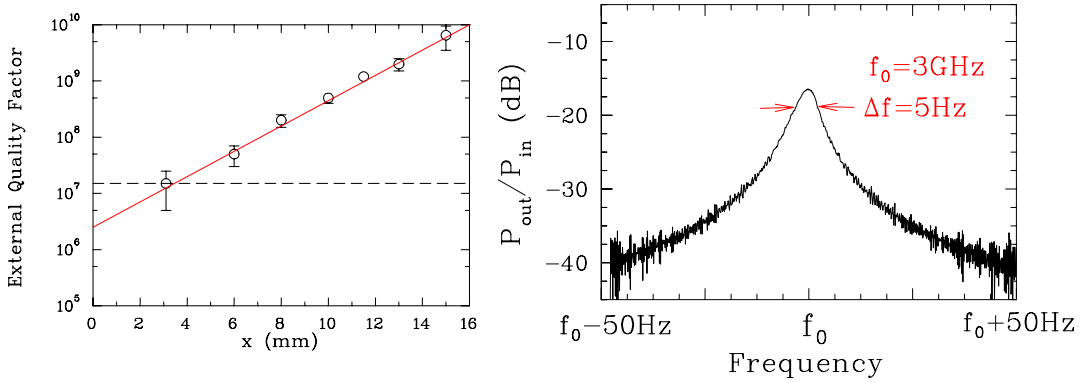

Fig. 19: Variable coupling strength and matched coupling without beam

In a low-energy electron accelerator like the S-DALINAC the beam is not yet completely relativistic and therefore the time needed for one recirculation still slightly depends on energy. On the other hand at the entrance of the main linac the injection phase has to be the same for all three beams. Thus it is necessary (since the accelerator has to provide a wide range of beam energies) to match the lengths of the recirculating beam transport systems for each beam energy. Figure 20 shows how this is done at the S-DALINAC. The encircled parts of the layout (blown up in the insets) indicate where the path length adjustment is performed.

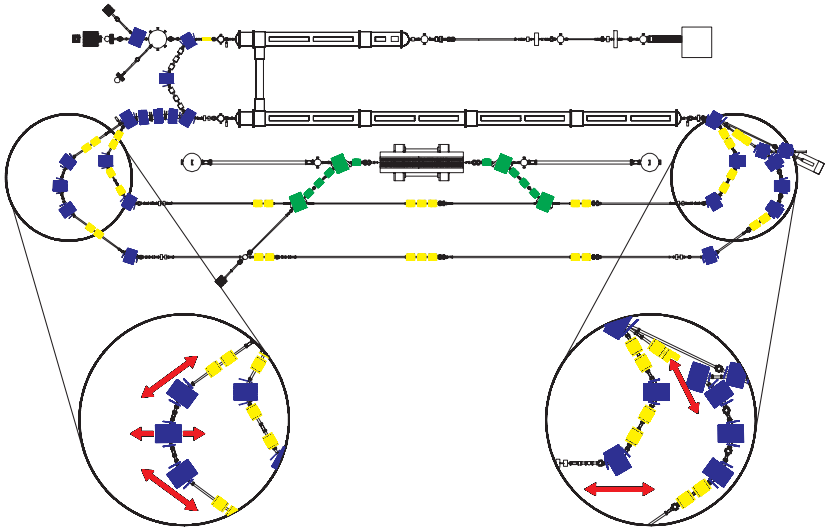

Fig. 20: Path length adjustment in the recirculating beam lines

In the first recirculation two dipole magnets and two quadrupoles (due to modified beam optics, there is now only one quadrupole between the two dipoles) are shifted on linear bearings in the direction of the arrows, allowing for a path length variation of 50 mm, corresponding to 180° of the

RF phase. For the second recirculation (left inset in Fig. 20) a length variation of ΔL = 62 mm (220° of RF phase) is achieved by shifting three dipoles in the indicated directions.

Since good diagnostics is important for the operation of any accelerator a few examples are discussed below to show how transverse and longitudinal properties of the electron beam are determined at the S-DALINAC. Measurements of the transverse intensity distribution of the beam have to be performed for a quantitative analysis of transverse beam parameters. For this purpose either wire scanners, giving projections of the intensity distribution, or CCD cameras, taking an image of the beam via Optical Transition Radiation (OTR) are used. A typical OTR diagnostics set-up is shown in Fig. 21.

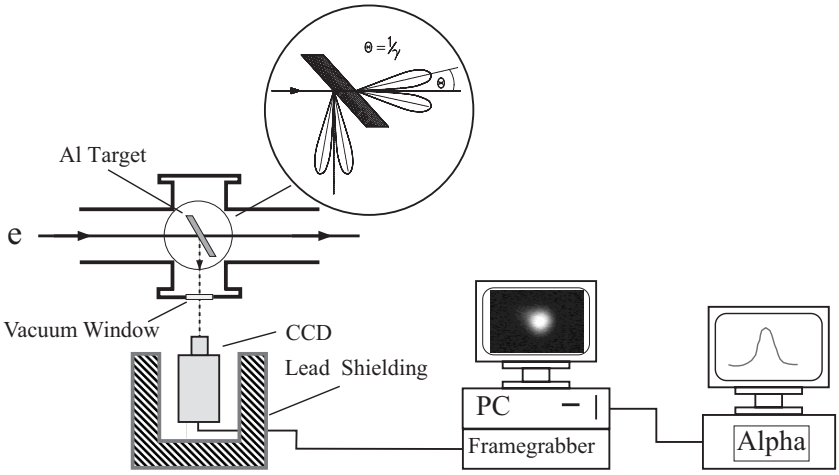

Fig. 21: Schematic set-up of an OTR diagnostics station

The inset in Fig. 21 shows the typical emission characteristics of OTR. The radiation produced by the electron beam hitting a 25 μm thick aluminum target is observed through a standard vacuum window by a well-shielded CCD camera, whose output is digitized in a PC equipped with a framegrabber board. Final analysis is performed on a workstation using IDL [4] as dedicated software. OTR is used for diagnostic purposes at energies ranging from as low as 250 keV up to 120 MeV requiring a minimum beam current of 0.5 μA down to 10 nA, respectively. Results from a typical measurement of transverse beam parameters (injector beam at 5.4 MeV) are displayed in Fig. 22, where the left part shows the two-dimensional intensity distribution of the beam on the aluminum foil (the original is a false colour presentation). The right part of Fig. 22 shows the horizontal half-widths of different intensity distributions obtained by variation of the focusing strength of a quadrupole, located upstream of the diagnostics station. A three parameter fit to the data yields the beam parameters and thus as the usually quoted global quantity the horizontal emittance given in Fig. 22.

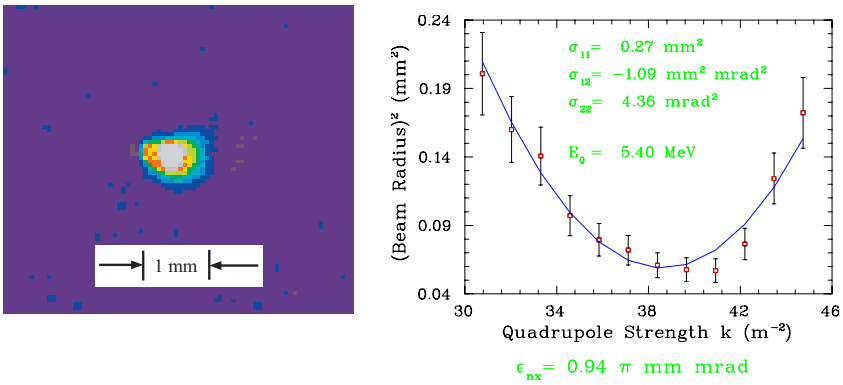

Fig. 22: Determination of transverse beam parameters via OTR

Determination of the transverse intensity distribution of the electron beam in a dispersive section of the lattice contains information on the energy spread of the beam. Results from such a measurement, taken from the beam after leaving the main linac, are displayed in Fig. 23. The two

intensity distributions shown in the left part of the figure correspond to an optimized (left picture) and a non-optimized (right picture) setting of the RF phases in the main linac. The right part of Fig. 23 shows a quantitative on-line display of the measured data: the intensity distribution is projected onto an energy scale and a Gaussian fit with its corresponding half-width are displayed to help the operator in an optimization process.

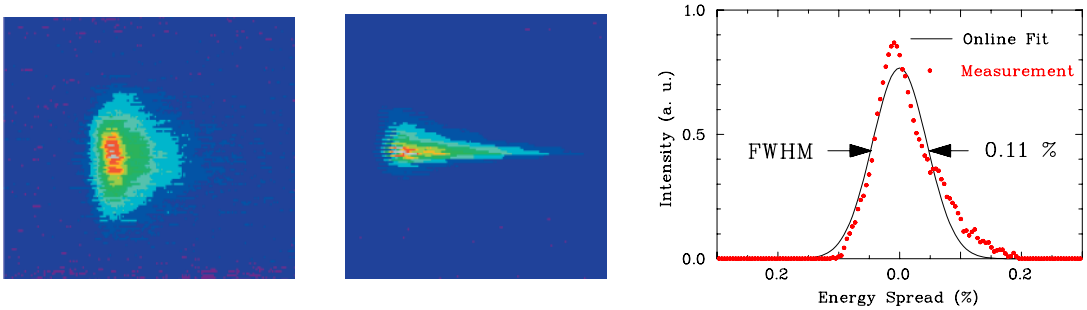

Fig. 23: Determination of energy spread via OTR

Knowledge of the bunch length and thus the peak current is essential for operation of the FEL. The apparatus shown in Fig. 24 (known as the Martin Puplett Interferometer [5]) makes use of the coherent Far InfraRed (FIR) part of transition radiation (the radiation is coherent for wavelengths comparable to or longer than the electron bunch length). A parabolic metal mirror deflects the radiation emitted from the aluminum foil onto a wire grid, which acts as a polarizer. The part of FIR radiation that is polarized perpendicularly to the plane of the drawing is deflected to the right onto a second wire grid, oriented under 45° with respect to the direction of polarization, thus acting as a beam splitter. The split parts of the radiation hit a fixed (top) and a moveable (right) roof mirror that rotate the direction of polarization by 90°. The FIR radiation is then recombined by the beam splitter and has a direction of polarization that depends on the position of the moveable mirror. A second parabolic mirror directs the radiation onto a third wire grid (analyser), from where the part to be detected is reflected into the feed horn of a pyroelectric detector.

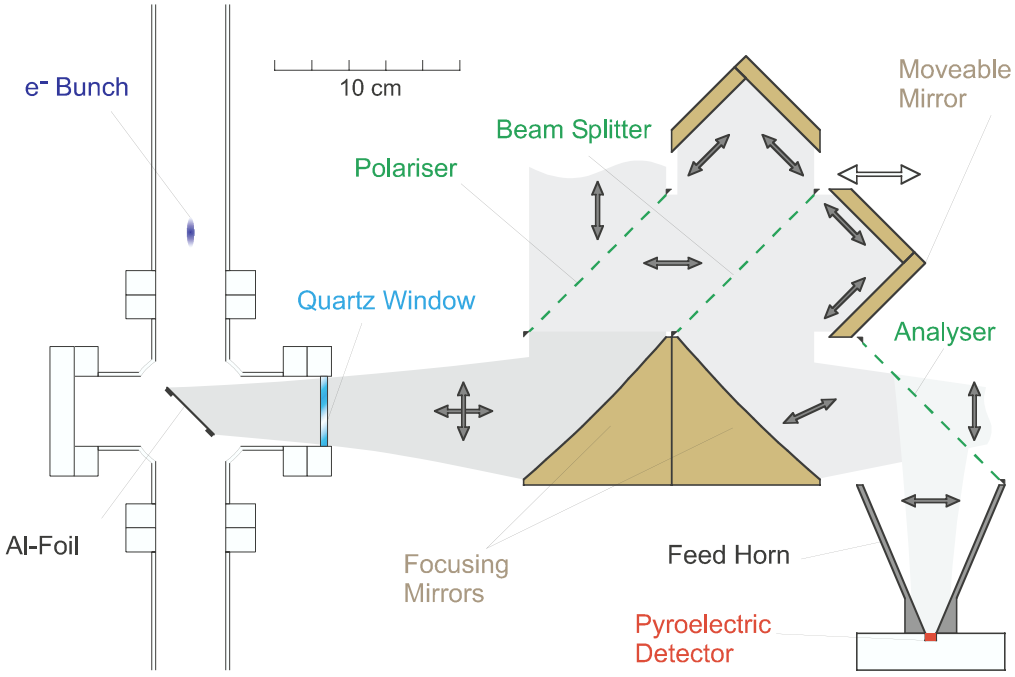

Fig. 24: Interferometer for the FIR part of transition radiation

The response of the detector (autocorrelation) as a function of the mirror position, expressed as optical path difference and converted into picoseconds, is drawn in the left part of Fig. 25. It has to be deconvoluted with respect to the very structured spectral response of the apparatus (including the

detector). The final result, the longitudinal intensity distribution of the electron bunch is shown in the right part of Fig. 25 (electron beam parameters are given in the inset).

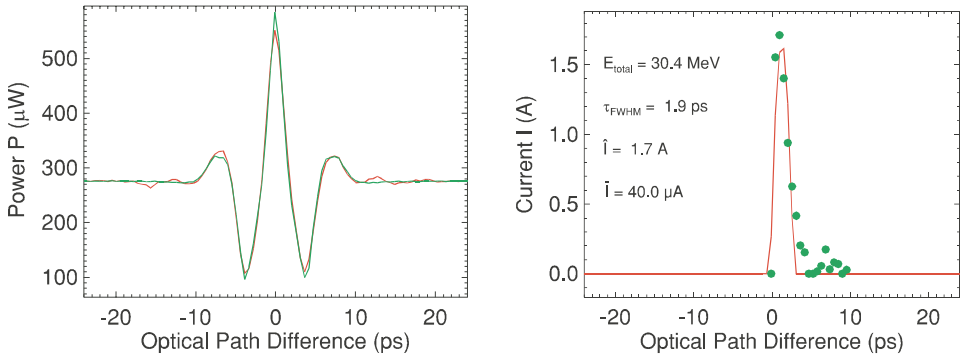

Fig. 25: Measured autocorrelation and corresponding bunch shape

For non-interceptive diagnosis of beam intensity and position RF cavity monitors in the TM_{010}- and TM_{110}-like modes are used. The cavities (a pair is shown in Fig. 26 with the associated electronics) are fabricated from stainless steel. They consist of a common centrepiece and two lids, sealed with copper gaskets. On the outside, the lids allow for a direct connection to standard CF 38 vacuum flanges. The antennas, four on the position monitor and two on the intensity monitor, are connected to 3.5 mm RF connectors through ceramic 50 Ω vacuum feedthroughs welded onto CF 16 flanges.

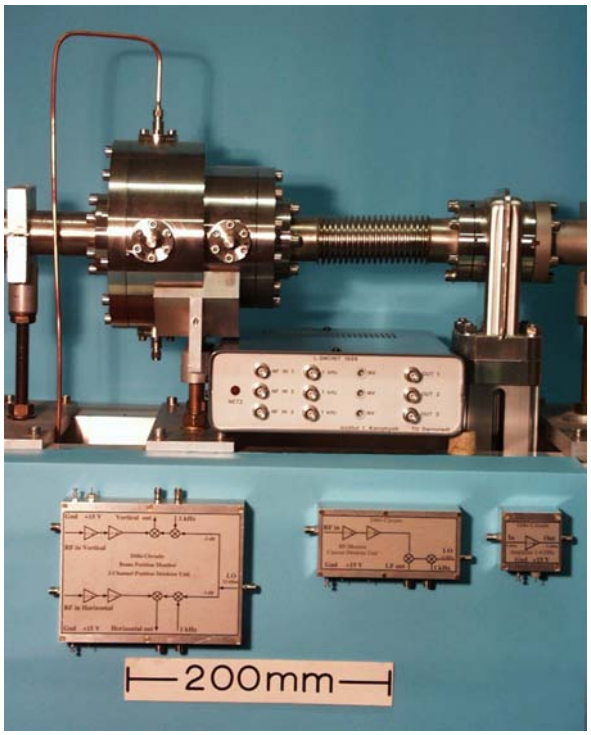

Fig. 26: Beam position and intensity monitors with associated electronics

The cavities have low quality factors ($Q \leq 10^3$), therefore only initial frequency tuning (after fabrication) is necessary and no special temperature stabilization is required. The resulting rather low RF sensitivities (15 nW/(μA)^2 for the intensity monitor and 15 pW/(mm·µA)^2 for the position monitor) are compensated for by the lock in detection technique, resulting in typical resolutions of 10 nA for the beam current and 0.1 mm for the beam position at a current of 1 μA.

4.1.3 CEBAF at TJNAF

CEBAF at TJNAF represents the high-energy end of CW electron accelerators for nuclear physics. A layout of the facility is sketched in Fig. 27 with design specifications for energy, current, emittance, and energy spread of the electron beam.

The electron source of the accelerator (left part of Fig. 24 on top of experimental hall A) produces a polarized 100 keV beam from a strained GaAs photocathode. After a special preparation of the bunch sequence, described below, the beam is accelerated to 500 keV in a 1.5 GHz CW normal conducting accelerating structure before it enters the superconducting injector linac. The superconducting accelerator cavities of CEBAF, originally developed at Cornell University, are 5-cell cavities fabricated from solid niobium, operating at 1.5 GHz. A pair of cavities, assembled head to head (with their RF input couplers in the centre) form a cryounit, which has its own helium vessel. Four such cryounits assembled together form a cryomodule (one cryostat). The injector linac consists of one cryounit (with a special cryostat) and two standard cryomodules. It accelerates the beam to 45 MeV. The main accelerator consists of two linacs that each contain 20 cryomodules (160 cavities). Between successive cryomodules beam diagnostics stations, quadrupoles, and vacuum pumps are installed. The nominal energy gain of each linac (which is exceeded in the meantime) is 400 MeV. After leaving the first linac the beam is deflected vertically in a so-called spreader section. The first pass (lowest energy) goes to the top level of the following 180° arc, is then deflected down to the linac level in a so-called recombiner section, and enters the second linac to gain another 400 MeV. In the same manner, in a second set of 180° arcs the beam is brought back to the entrance of the first linac for its second pass acceleration. Transition to the second linac is accomplished through the second arc from the top one in the set of five 180° arcs (right side of Fig. 27). Since there are four arcs contained in the left set the beam can pass up to five times through each linac. Each one of the nine 180° arcs is composed of many compact dipoles, quadrupoles, and sextupoles. Longitudinally, the beam transport is isochronous. The accelerator serves three experimental halls, A, B, and C (left part of Fig. 27) and it is the very special property of CEBAF that beam can be delivered simultaneously to all three halls, even at different energies and intensities.

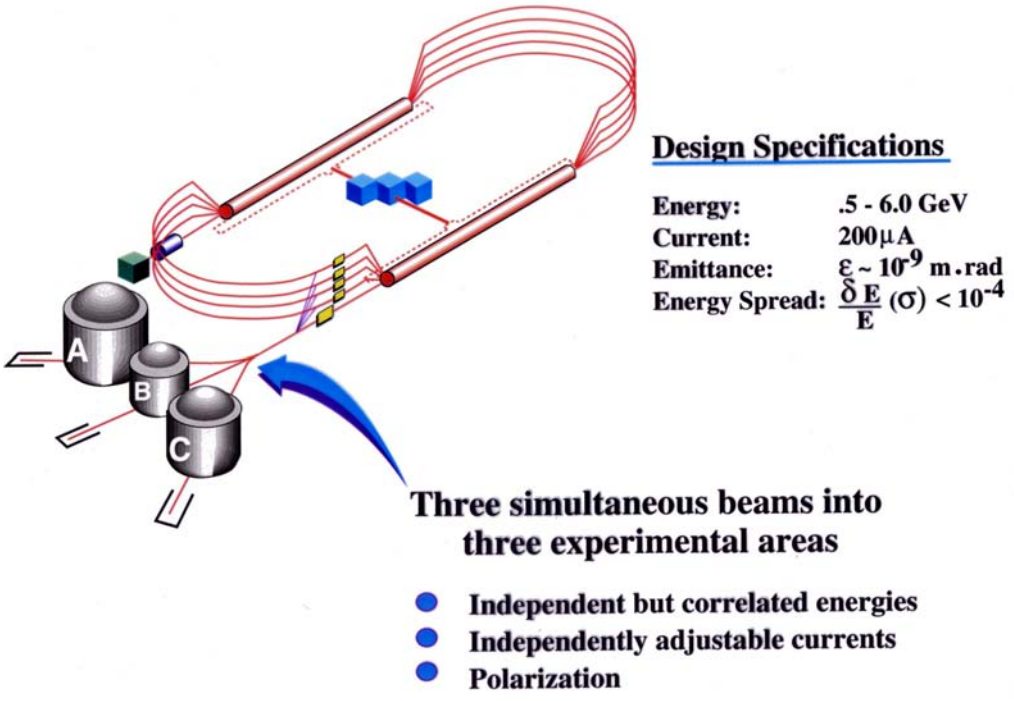

Fig. 27: Layout of CEBAF at TJNAF

The way this is accomplished is illustrated in the following two figures. The principle of basically accelerating three individual beams in the same accelerator is sketched in Fig. 28. It requires, to some extent, individual preparation of successive electron bunches. For example, in the case of CEBAF only every third bunch is identical. This is indicated by the empty, dotted, and full small circles in Fig. 28.

The second requirement is that one must find a way to direct only every third bunch to the same experimental hall and to extract the bunches in between after a different—or the same—number of passes through the accelerators, and to direct them to the other two experimental halls.

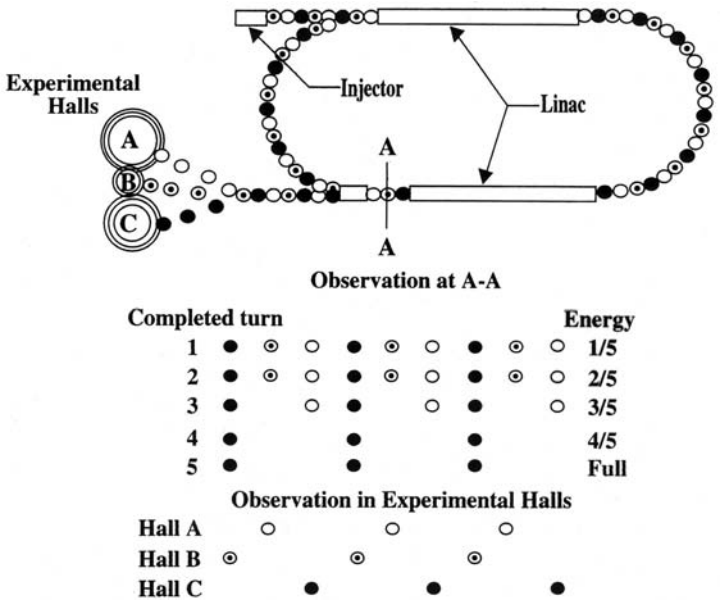

Fig. 28: Scheme of simultaneous beam delivery

Provided this is possible, a situation as sketched in the lower part of Fig. 28 can be achieved: the injector periodically prepares a sequence of three bunches with different charge. At the exit of the second linac (location A-A) the bunches pass in the same periodic order as they leave the injector. After the second pass the dotted bunches, for example, are extracted to hall B and thus are missing at A-A. If the bunches indicated by empty circles are then extracted to hall A the last two passes contain only the full-circle bunches, to be directed finally to hall C at maximum energy. In this case each hall gets its own beam of individual intensity (determined by the preparation in the injector): hall B at 2/5 of the full energy, hall A at 3/5, and hall C at full energy.

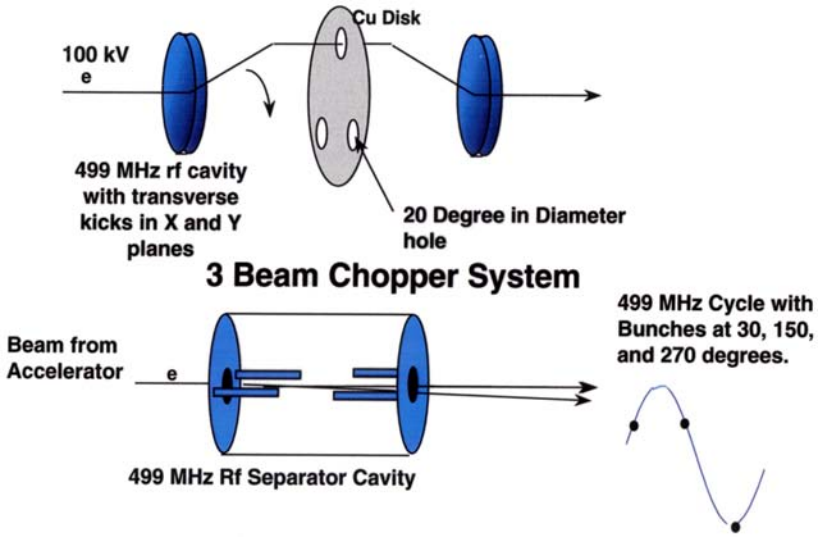

Fig. 29: Generation and separation of three independent beams

The upper part of Fig. 29 shows how (periodically) the individual bunches are prepared in the injector. The 100 keV beam from the electron gun is deflected transversely by an RF cavity which operates at 1/3 of the accelerator frequency. Deflections in the x and y direction are out of phase by

90°, i.e. the beam is deflected tangentially to a cone. If this beam hits the Cu disc with three holes, indicated in Fig. 29, three packets of electrons will pass through the disc while the beam performs one round trip on the cone. The Cu disc is surrounded by a solenoidal lens, which bends the electron packets back towards the original beam axis, where a second RF cavity brings the packets back on axis. Each packet fits into one RF bucket of the accelerator, since the deflection was performed at one-third of the accelerator frequency. Different intensities in the three packets can be achieved either by modulating the laser that illuminates the photocathode properly (in this case the diameter of the holes in the Cu disc are just limiters for the duration of the electron packets) or by replacing the three holes with adjustable slits (the width of the slits determines the charge contained in the electron packets). Extraction of the individual bunches after (partial) acceleration is more difficult because of the increased electron energy, but the first device is again an RF cavity operating at one-third of the fundamental frequency. This cavity is a true separator cavity, consuming a significant amount of RF power and deflecting the beam in one direction only. The right part of Fig. 29 shows that for a certain phasing of the separator two successive bunches are deflected to one side by the same amount, while the third bunch is deflected more strongly to the opposite side. The RF separator is followed by a series of septum magnets to finally direct the individual bunches into the different extraction beam lines.

Despite producing data at an impressive rate, the TJNAF has already studied upgrade possibilities very carefully. The version currently preferred is shown in Fig. 30. The important modifications necessary for the upgrade are listed in the top left of the figure and are indicated in the sketch of the accelerator: five additional cryomodules with newly developed 7-cell cavities must be installed behind each linac. Six of the installed cryomodules must be replaced or reworked. The capacity of the helium refrigerator has to be increased to 10 kW. Magnets and power supplies have to be replaced in the 180° arcs and in the spreader and recombiner sections.

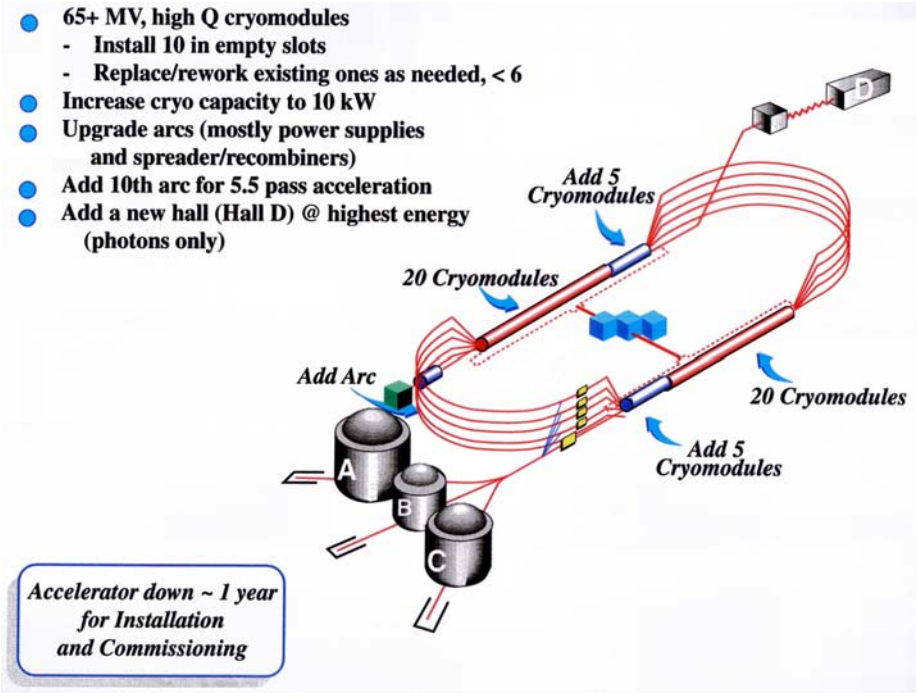

Fig. 30: Proposed upgrade to CEBAF at TJNAF

These modifications are supposed to increase the beam energy for the existing three experimental halls to 10 GeV. For photon experiments at energies up to 12.5 GeV a fifth arc in the left arc section, allowing for a sixth pass through the first linac, and a fourth end station (top right) are proposed.

4.1.4 ELFE at CERN

An Electron Laboratory For Europe (ELFE) significantly exceeding even the energy of the CEBAF upgrade has been under discussion for several years. Following a first study at CERN [6], CERN and NuPECC set up a joint study for ELFE at CERN, a superconducting recirculating 25 GeV electron accelerator that would use the superconducting accelerator cavities of LEP II and other components not required for LHC. In parallel an international study group at CERN looked into the design aspects of such an accelerator and in December 1999 a conceptual design report [7] was published.

A schematic view of ELFE at CERN is shown in Fig. 31 and a brief summary of its main parameters is given in Table 4.

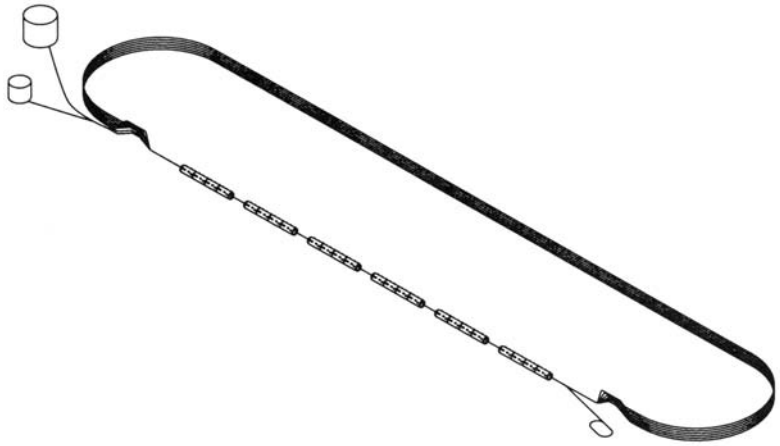

Fig. 31: Schematic view of the ELFE accelerator

ELFE will use a polarized electron source (semiconductor photocathodes as in MAMI and CEBAF). Two scenarios have been investigated for the injector: a two-stage, normal conducting racetrack microtron (very similar to MAMI B, except for two stages instead of the three at MAMI B), or a superconducting recirculating accelerator with two recirculations (quite similar to the scheme of the S-DALINAC). Both injectors have to provide 800 MeV of beam energy. Different from CEBAF, ELFE will use one linac only in its recirculation scheme. Its energy gain will be 3.5 GeV and thus seven passes of the electron beam through the linac are needed to achieve the final energy of 25 GeV. The arcs of the return lines for the beam are arranged in a similar scheme as in CEBAF (on top of each other, with the same radius) but there is only one spreader section (at the exit of the main linac) and one recombiner section (in front of the main linac). Therefore, six straight return lines (parallel to the main linac and on top of each other) are necessary in this recirculation scheme.

Table 4: The most important ELFE design parameters

Top energy	25 GeV
Beam current on target	100 μA
Bunch separation on target	2.8 ns
Injection energy	0.8 GeV
Number of passes	7
Energy gain per pass	3.5 GeV
Relative r.m.s. momentum spread	$\leq 10^{-3}$
Emittance	$\leq$ 30 nm

The first two figures in Table 4 show the enormous amount of beam power (2.5 MW in the case of ELFE) that hits the target in such a high energy nuclear physics accelerator. The fairly large bunch separation of 2.8 ns is of course due to the low operating frequency of the LEP cavities (350 MHz) typical of storage rings. The estimated capital expenditure for the construction of ELFE at CERN amounts to some 400 MCHF, split equally between accelerator components and conventional construction.

4.2 Superconducting electron linacs

The next generation of accelerators providing colliding beams of electrons and positrons at energies in the TeV regime will be linear colliders, two linacs directed from opposite directions at a common interaction point. In order to reach the necessary luminosity (required by the small cross sections at TeV energies) bunch charges of several nC and thus extremely high beam power are required. As a consequence linear colliders are pulsed accelerators with a duty factor of the order of one per cent or less. Traditionally this has been the domain of normal conducting linacs and (as discussed in Section 2) the advantages of superconducting linacs are most obvious for CW accelerators. Detailed studies, however, have shown that superconducting cavities, which provide good power efficiency and can be operated at comparably low frequencies, are very likely the superior choice for a linear collider. They are preferable because of the strongly reduced excitation of wakefields. Since about a decade the feasibility of TESLA has been investigated and, centred at DESY, an international collaboration has worked on the layout of TESLA [8] and established the TESLA Test Facility to demonstrate that such an accelerator can be built, to push superconducting accelerator technology to its limits, and to find the most reliable and cost-efficient way for the construction of a superconducting linear collider.

A schematic layout of the TESLA linear collider is shown in Fig. 32. A train of low-emittance electron or positron bunches is extracted from a source system, compressed longitudinally, and injected into two opposing linear accelerators at an energy of 10 GeV. The bunches are carefully aligned along the accelerator axis as defined by the RF cavities and the quadrupole magnets and are accelerated to 250 GeV in each linac. After acceleration the beam halo is removed by a set of precision collimators, and the bunches are transported and focused down to a few hundred nanometres in the horizontal direction, and to the order of 10 nm in the vertical plane, and are collided head-on. The large bunch spacing (compared with normal conducting linear colliders) allows the use of a bunch-to-bunch feedback system, necessary to ensure that opposing bunches collide head-on at the interaction point. The spent beams are extracted from the interaction region and are either dumped (positrons) or used (electrons) to produce the next batch of positrons.

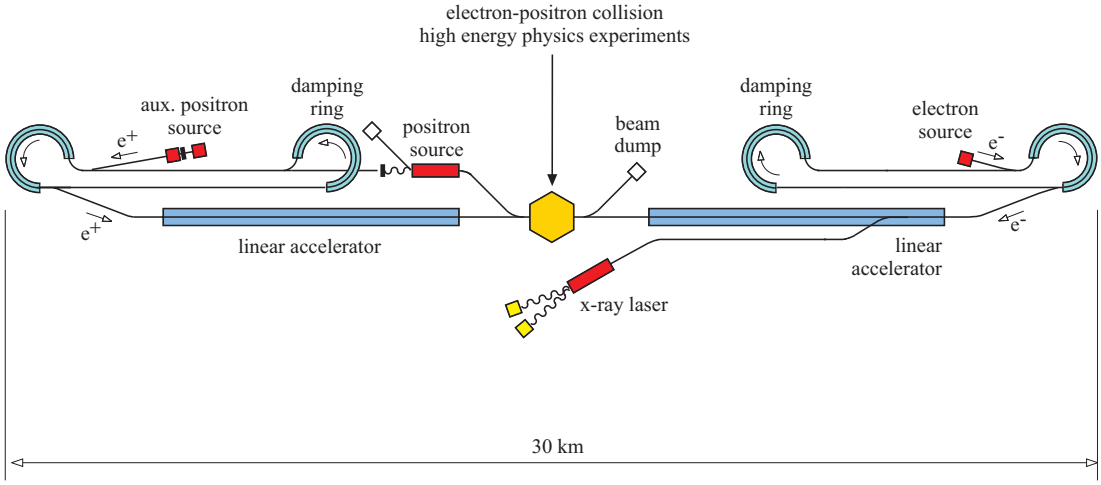

Fig. 32: Schematic layout of TESLA

Interleaved with the bunches for particle physics, bunches of electrons originating from a low-emittance RF photocathode gun are longitudinally compressed and accelerated to energies of between 10 and 50 GeV. They are then extracted from the linac and passed through long, high-precision undulators. The low-emittance electron bunches traversing the undulators will yield a very bright, very short burst of transversely coherent light with tunable wavelengths in the sub-nanometre region. Using

a transverse mode cavity to deflect the beam it is possible to feed several undulators during the same RF pulse, and consequently such a facility can serve a large number of users without interfering with the particle physics programme.

Some of the most important parameters of the 500 GeV linear collider TESLA 500 and of the (original) TTF Linac (TTFL) are summarized in Table 5. A comparison of the figures for the TTFL and for TESLA 500 shows that the most important criteria for the big machine have yet to be demonstrated in the test facility.

Of course, the beam energy is much lower and the number of cryomodules is much smaller in the TTFL, but the 9-cell superconducting cavities developed for TESLA (which in the meantime have become the standard for superconducting cavities) were expected to operate at 15 MV/m and to demonstrate that 25 MV/m for TESLA were not unrealistic. Due to numerous improvements in quality control, fabrication procedures, treatment, handling, and assembly of the cavities a gradient of 25 MV/m is presently already regarded as a standard. Also an unloaded Q-value of 5×10^9 is quite usual for the TESLA cavities. The first injector in TTF used a thermionic source with a bunch charge of a few 10^8 electrons per bunch with a much higher bunch repetition rate. Since then, a photocathode in an RF gun has been used as the source. This provides the same bunch charge and repetition rate as will be used in TESLA 500.

Table 5: Comparison of parameters for TTFL and TESLA 500

Parameter		**TTFL**	**TESLA 500**
Main linac			
Energy	(GeV)	0.500	250
RF frequency	(GHz)	1.300	1.300
Accel. gradient	(MV/m)	15/25	25
Q_0		3×10^9	5×10^9
Cryomodules		4	2500
Injector			
Energy	(GeV)	0.020	10
Particles/bunch		5×10^{10}	5×10^{10}
Bunch separation	(μs)	1.0	1.0
Macro pulse length	(μs)	800	800

In the course of its development and construction the layout of the TTFL was modified with respect to its original design [9]. The present configuration is sketched in Fig. 33.

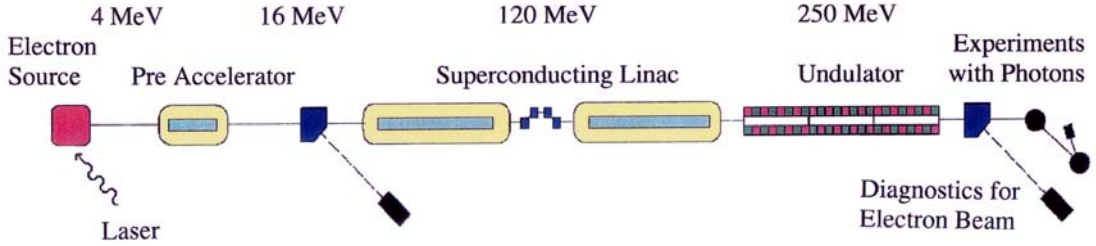

Fig. 33: Layout of the TESLA Test Facility Linac

The tunable X-ray laser envisaged for TESLA is based on the principle of Self-Amplified Spontaneous Emission (SASE) as there are no mirrors available for an optical cavity in the sub-nanometre wavelength range. In order to prove that the SASE principle works at very short wavelengths the number of cryomodules for the TTFL was reduced and a very precise 15 m long undulator was installed downstream of the linac with the necessary diagnostics for the electron beam and the generated laser radiation. First experiments with the configuration (shown in Fig. 33) were successful in the spring of this year; the expected development of the installation is discussed in Section 4.3.

4.3 Superconducting linacs driving an FEL

Free-Electron Lasers require fairly high peak currents, usually provided by short bunches and high bunch charges. Electrostatic accelerators as well as normal conducting and superconducting linacs are used as drivers. For FELs operating in a CW mode superconducting linacs are the only choice (except at low energies where electrostatic accelerators can be used). The basic principle of a conventional FEL is illustrated in Fig. 34. The electron beam from the accelerator is directed through an undulator, which provides a periodically alternating magnetic field (the length of the magnetic period being λ_u). In Fig. 34 the undulator field is oriented horizontally and the electrons perform vertical oscillations about their reference trajectory while passing through the undulator. At the same time they emit synchrotron radiation (spontaneous radiation) that, for small amplitudes of the oscillatory motion, consists of a line spectrum rather than the usual continuous synchrotron radiation spectrum.

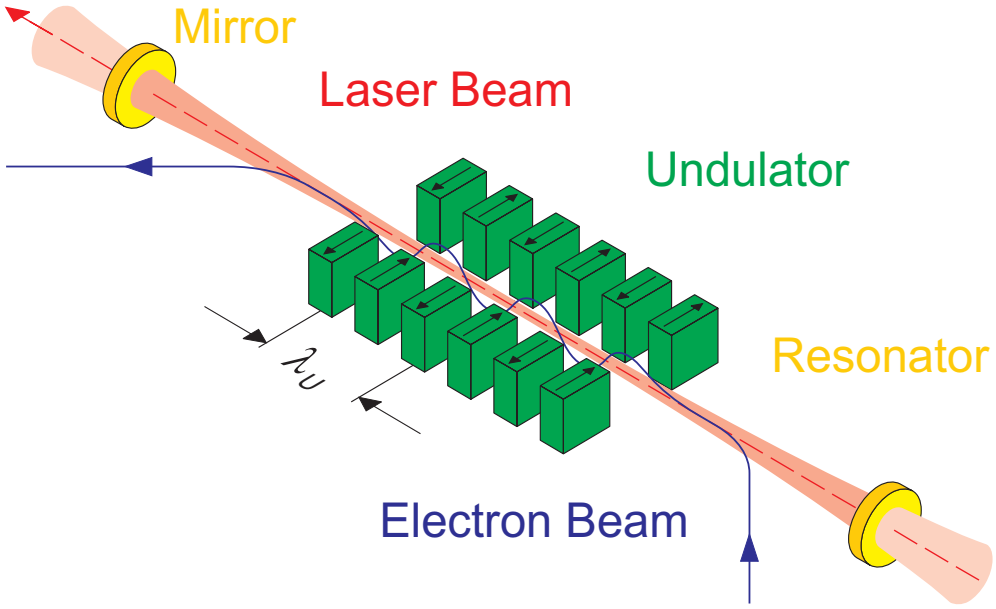

Fig. 34: Principle of conventional free-electron lasers

The fundamental wavelength λ of the spontaneous radiation is given by $\lambda = (\lambda_u/2\gamma^2)(1 + K^2/2)$ with K, the undulator parameter, containing the magnetic properties of the undulator ($K \approx 1$). The pulse of spontaneous radiation generated by an electron bunch while passing through the undulator travels down the optical cavity, is reflected by the downstream (left) mirror, and hits the upstream (right) mirror where it is reflected again. If the length of the optical cavity (distance between the two mirrors) is adjusted correctly the pulse of spontaneous radiation when passing through the undulator from right to left will overlap with the successive electron bunch. Due to their oscillatory motion in the undulator region the electrons can transfer energy into the electromagnetic field of the spontaneous radiation. This amplification for one round trip of the spontaneous radiation is called small signal gain and depends among other parameters on the peak current of the electron beam. If the small signal gain exceeds the losses inside the optical cavity the intensity of the spontaneous radiation increases with each round trip until the laser finally (due to limiting processes) reaches saturation. The laser radiation is coupled out through one of the mirrors; in the case of dielectric mirrors by using one mirror with the

appropriate transmission, in the case of metallic mirrors by a hole of appropriate size in the centre of one mirror.

The rather high peak current necessary to drive an FEL population of each successive RF bucket in a superconducting linac with an electron bunch would result in excessive beam power and demand for RF power. The situation at the S-DALINAC (Fig. 35) illustrates this fact in a most impressive way.

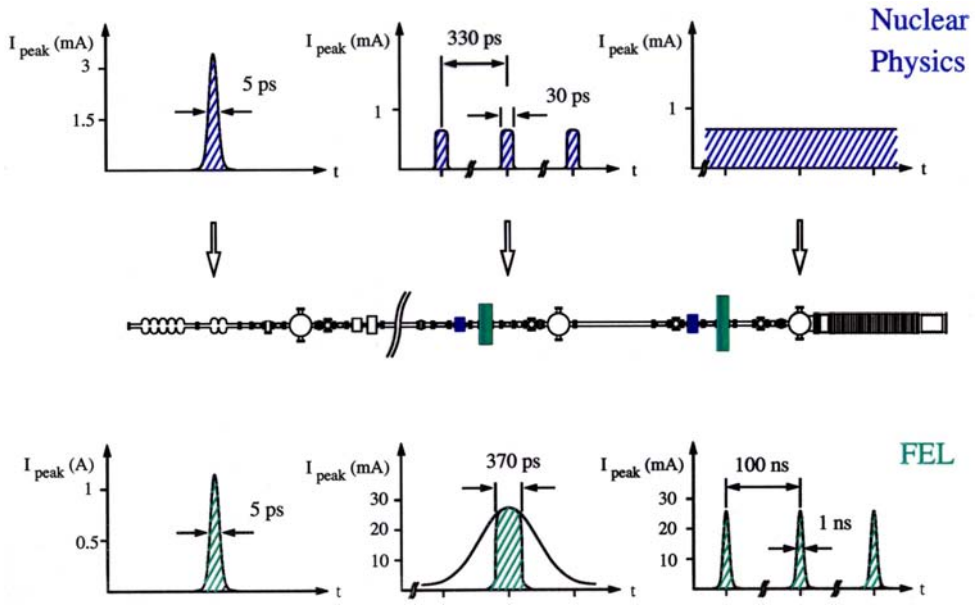

Fig. 35: Time structure for nuclear physics and for FEL operation

Each accelerating cavity has its own small RF transmitter and can provide 300 W for acceleration of the beam. At an energy gain of 5 MeV in the 1 m long cavity this corresponds to a maximum average beam current of 60 μA. Considering a bunch length equal to two degrees of RF phase, the maximum peak current amounts to 10 mA if every RF bucket is populated, which is the case when the accelerator is used for nuclear or radiation physics experiments. The FEL, however, in order to provide enough small signal gain for lasing operation, requires a peak current of some 3 A. This can only be achieved by increasing the bunch charge by a factor of 300 and consequently populating only every 300th RF bucket (thus staying below the RF power limit).

To allow for this type of operation a pulsing option for the electron gun, operating at a repetition rate of 10 MHz (300th subharmonic of the accelerator frequency) and a 600 MHz (5th subharmonic) chopper/prebuncher system had to be incorporated into the 250 keV injection of the accelerator. The central part of Fig. 36 displays a schematic layout of the modified injection, consisting (from right to left) of a 10 kV thermionic gun, a 250 kV electrostatic preaccelerator tube, a 3 GHz chopper/ prebuncher system for nuclear physics operation, a 600 MHz chopper/prebuncher system for FEL operation, chopping aperture, and the superconducting 2-cell and 5-cell capture sections.

Figure 36 shows the time structure of the electron beam at the locations indicated by the arrows for the two modes of operation. For nuclear physics experiments the chopper cavity and the water-cooled chopper aperture chops the DC current from the electron gun into pulses of 30 ps. The prebuncher cavity compresses the width of these pulses to 5 ps at the entrance of the capture section of the superconducting injector linac. Since the beam is both accelerated and bunched in the capture sections, the bunch length is further reduced to 2 ps at the end of the injector.

For FEL operation the 1 ns wide pulses from the electron gun are chopped to a width of 370 ps by the 600 MHz subharmonic chopper and the chopper aperture. The subharmonic prebuncher then compresses the pulse width again to 5 ps at the entrance of the capture section. Similar to the 3 GHz CW operation, the capture sections reduce the bunch length to 2 ps while increasing the peak current. Thus, the peak current corresponding to the emitted electron current of 27 mA from the gun amounts to 2.7 A.

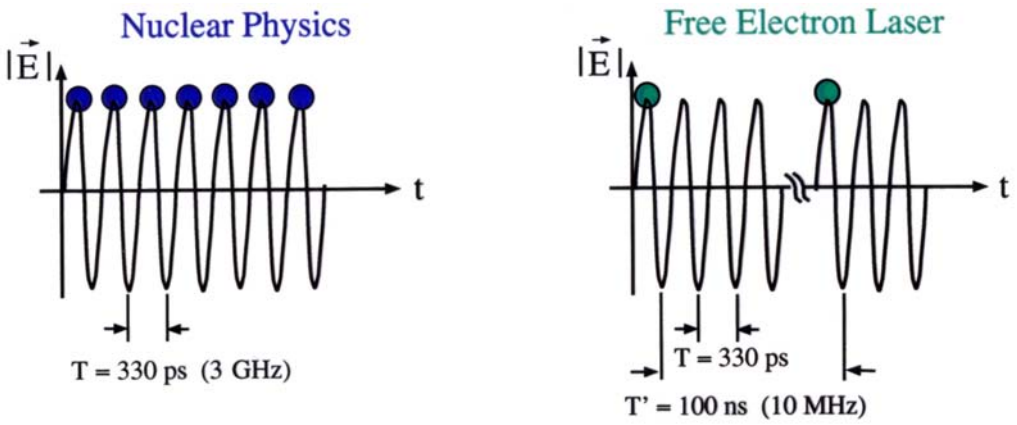

Fig. 36: Time structure of the beam for nuclear physics (3 GHz CW) and FEL (10 MHz CW) mode of operation

The difference between spontaneous radiation at the very beginning of the FEL start-up and the laser radiation during saturated operation is shown in Fig. 37, which displays the spectra for the two conditions.

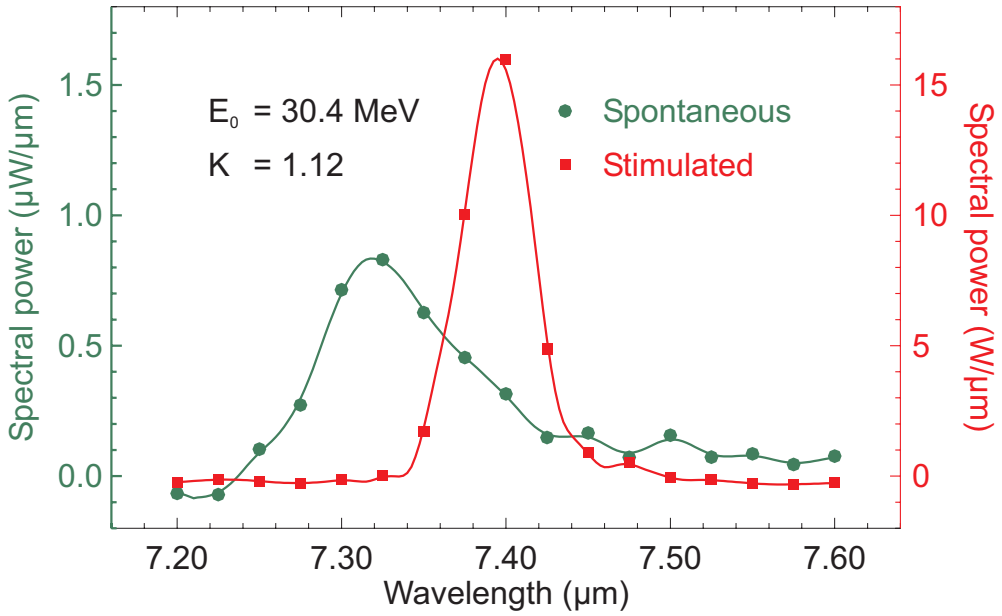

Fig. 37: Spectra of spontaneous (left ordinate) and laser radiation (right ordinate) from the S-DALINAC FEL

The spectral power displayed on the ordinate axes (left axis for spontaneous radiation, right axis for stimulated radiation) increases by more than seven orders of magnitude, in agreement with the fact that some 10^7 electrons in a bunch emit coherently in stimulated emission. Another fact is also beautifully displayed by Fig. 37: according to FEL theory (Madey's Theorem) the spectral width of the spontaneous radiation is reduced by a factor of two in the case of stimulated emission.

Presently the most powerful (average power) FEL is the IR DEMO at TJNAF. The installation (roughly sketched in Fig. 38) uses a 350 kV electron gun with a laser-driven photocathode. The superconducting injector linac consists of a short cryomodule, housing two CEBAF 5-cell cavities. The injector produces a 10 MeV beam with an r.m.s. energy spread of 15 keV, the bunch length amounts to 2 ps and bunch repetition frequencies ranging from 4.7 to 74.8 MHz can be provided. The linac currently consists of a standard CEBAF cryomodule equipped with eight 5-cell cavities. It provides an energy gain of 38 MeV. The beam after leaving the linac is passed around the upstream mirror of the optical cavity and the bunch length is magnetically compressed to 0.4 ps before the beam is directed through the undulator (wiggler).

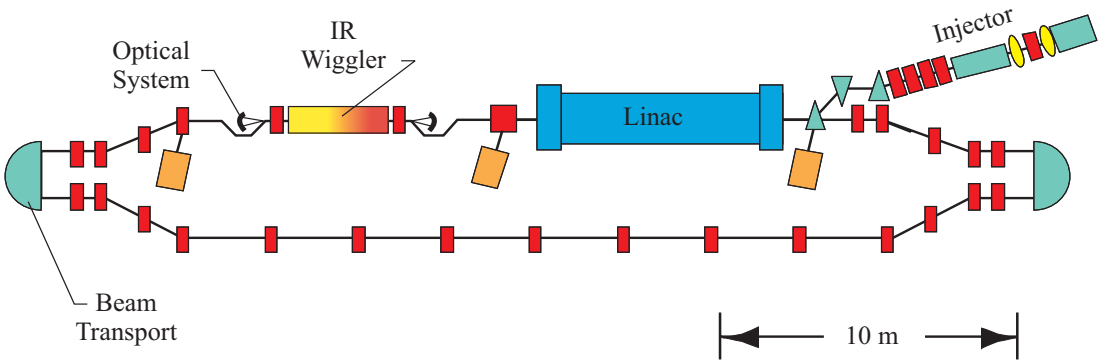

Fig. 38: Layout of the IR DEMO FEL at TJNAF

After passing the undulator and the downstream mirror of the optical cavity the electron beam can be recirculated by means of a very carefully designed beam transport system. In the case of the IR DEMO FEL the purpose for recirculating the beam is *not* to accelerate it one more time, but to decelerate the beam to 10 MeV and return the energy it draws from the linac cavities during its acceleration directly back to the RF field in those cavities. The beam is dumped at an energy of 10 MeV after its second passage through the linac following separation from the first pass beam by a magnetic chicane. Because, after passing the undulator, the electron beam has an r.m.s. energy spread of 2 MeV, it covers large transverse dimensions in dispersive sections of the recirculation system. An isochronous recirculation would leave the energy spread of the beam unaltered, even after deceleration, i.e. the 10 MeV beam would still have an r.m.s. energy spread of 2 MeV. Therefore transverse and longitudinal properties of the recirculation system have been carefully designed, including higher order corrections. As a result the decelerated beam leaves the linac with an r.m.s. energy spread of 0.5 MeV and can be dumped easily. The IR DEMO FEL has beautifully shown that this energy recovery scheme works almost perfectly. A beam current of up to 5 mA has been accelerated, producing an infra red beam with 1.7 kW of average power. At the same time it was demonstrated that in the energy recovery mode of operation the amount of RF power necessary to excite the linac cavities to their respective gradients did not depend on the beam current, whereas without energy recovery acceleration of 1 mA of beam current doubled the linac cavities' RF power consumption. The injector linac of course has to provide the full power necessary to accelerate the 5 mA beam to 10 MeV.

The SASE FEL of the TTF at DESY in its present configuration (displayed in Fig. 33) has successfully demonstrated that an FEL based on the SASE principle works in the UV wavelength region. Laser operation with a single pass gain of $G \approx 1000$ was achieved in the 80–180 nm wavelength range. This shows that long undulators with the extreme precision required by a SASE FEL can be built and that the transverse position of the electron beam can be controlled to within a few tens of μm.

Figure 39 indicates how the development of SASE FELs at DESY will continue. For phase one a third TESLA cryomodule with eight cavities will be inserted to increase the beam energy to 390 MeV. Two stages of bunch compression will reduce the bunch length to 250 μm. With the present undulator a laser beam of 44 nm wavelength, corresponding to a photon energy of 28 eV, will be produced. Then in a major upgrade of the facility (phase two) a third stage of bunch compression will be added at an energy of 390 MeV to reduce the bunch length to 50 μm. Five more TESLA cryomodules will then produce an electron beam of 1 GeV. The length of the present undulator will be doubled (necessary for the SASE principle to work at 1 GeV) and the laser beam generated by this facility will have a wavelength of 6 nm (200 eV photon energy). This source of continuously tunable coherent light in the VUV wavelength range with extreme brightness will of course become a true users' facility.

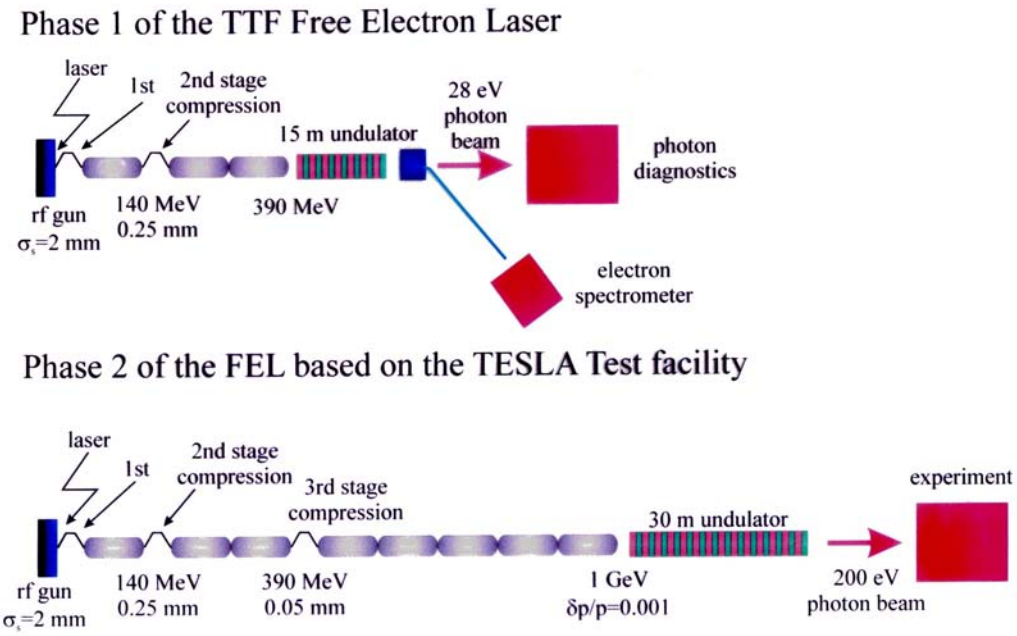

Fig. 39: Steps toward a 6 nm SASE FEL at DESY

5. CONCLUSION

First attempts to use superconducting RF structures for particle acceleration were undertaken at Stanford University and the Kernforschungszentrum Karlsruhe in the 1960s. The optimistic expectations from the new technology were inevitably followed by a few experimental drawbacks. It was only after some years of development that the first electron accelerators were assembled at the University of Illinois and at Stanford University, and the first superconducting booster for heavy ions became operative at Argonne National Laboratory. The S-DALINAC is historically the third superconducting electron linac. In the meantime the technology has matured. Superconducting RF structures have for many years been proven to operate not only in linacs but also in storage rings, even with extremely high beam currents, e.g. the Cornell B-factory. Large installations involving many cavities, like LEP II (some 200 cavities) or CEBAF (more than 330 cavities), have demonstrated the reliability of the technology. Therefore, old prejudices have disappeared; designs using superconducting technology are carefully studied and quite often appear to be the most effective and attractive solution for almost all big future accelerator projects, be they linear colliders, high-intensity proton accelerators, or accelerators for radioactive beams.

ACKNOWLEDGEMENTS

We are grateful to L.S. Cardman, S. Döbert, K.H. Kaiser, G.R. Neil, and H. Weise for generously providing us with information and material on the accelerators at their respective home institutions. In particular we are indebted to S. Kostial for his great help in the course of the preparation of the tutorial and this manuscript.

This work has been supported by the Deutsche Forschungsgemeinschaft under contract FOR 272/2-1 and the Graduiertenkolleg GRK 410.

REFERENCES

[1] H. Padamsee, J. Knobloch, and T. Hays, *RF Superconductivity for Accelerato* (John Wiley & Sons, New York, 1998)

[2] R. E. Rand, *Recirculating Electron Accelerators* (Harwood Academic Publishers, London, 1984)

[3] IKP Mainz (MAMI) Web page, http://www.kph.uni-mainz.de at the time of publication.

IKP Darmstadt (S-DALINAC) Web page, http://www.s-dalinac.de at the time of publication.

TJNAF (CEBAF, IR DEMO FEL) Web page, http://www.cebaf.gov/accel/index.html at the time of publication.

CERN (ELFE) Web page, http://hbu.home.cern.ch/hbu/Elfe/Elfe.html at the time of publication.

DESY (TTF, TESLA) Web page, http://tesla.desy.de at the time of publication.

[4] Interactive Data Language, Version 3.0, Research Systems (1993) 4.

[5] D.H. Martin, E. Puplett, *Inf. Phys.* **10** (1970) 105.

[6] G. Geschonke and E. Keil, 'A recirculating electron accelerator (ELFE) using the LEP superconducting RF cavities', CERN–SL–98–060–RF, CERN, Geneva (1998).

[7] H. Burkhardt (ed.), 'ELFE AT CERN, Conceptual Design Report', CERN 99–10, CERN, Geneva (1999).

[8] R. Brinkmann, G. Materlik, J. Rossbach and A. Wagner (eds.), 'Conceptual design of a 500 GeV e^+e^- linear collider with integrated X-ray laser facility', DESY Report 1997–048, ECFA Report 1997–182 (1997).

[9] D.A. Edwards (ed.), 'TESLA Test Facility linac—Design report', TESLA 95–01 (1995).